RSC Advances

ROYAL SOCIETY OF CHEMISTRY

www.rsc.org/advances

Conductive polymers/zeolite (nano-)composites: sub-exploited materials

Mehdi Jaymand*

* Correspondence to: Mehdi Jaymand, Research Center for Pharmaceutical Nanotechnology, Tabriz University of Medical Sciences, Tabriz, Iran

Tel: +98-411-3367914; Fax: +98-411-3367929.

Postal address: Tabriz-5165665811-Iran

E-mail addresses: m_jaymand@yahoo.com; m.jaymand@gmail.com; jaymandm@tbzmed.ac.ir

Abstract

In recent decades, there has been growing interest in the development of organic-inorganic hybrid materials in order to obtain new kind of materials with synergetic or complementary behavior for various practical and technological applications. Among the enormous kinds of these materials the conductive polymers/zeolite (nano-)composites represent a new class of materials system due to their novel physicochemical properties and potential for various practical and technological applications such as sensors, cathodes of the cells, anticorrosive, membranes, and selective removal of heavy metal ions from sea water and industrial waste waters. However, these materials were sub-exploited and there was only a few researches conducted for the preparation and application of conductive polymers/zeolite hybrids. This review provides a snapshot of recent progress in the synthesis, materials properties, and applications of conductive polymers/zeolite (nano-)composites reported until March 2014.

Contents

1. Introduction
2. Preparation methods of conductive polymers/zeolite (nano-)composites
3. Polyaniline/zeolite (nano-)composites
4. Polypyrrole/zeolite (nano-)composites
5. Polythiophene/zeolite (nano-)composites
6. Other conductive polymers/zeolite (nano-)composites
7. Summary and conclusion

Acknowledgment

References

Abbreviations

1. Introduction

It is a decisive fact that intrinsically conductive polymers (ICPs) have stimulated great interest on the basis of their importance in basic scientific research and potential industrial applications, due to their unique semiconducting and optoelectronic properties [1-12]. In particular, conjugated polythiophene (PTh), polypyrrole (PPy), polyaniline (PANI), and their derivatives stand out as the most promising members of the conjugated polymer family because of their unique electrical behavior, excellent environmental and thermal stability, low-cost synthesis, and mechanical strength [13-17]. These conducting polymers have potential applications in electromagnetic interference (EMI) shielding [18-22], rechargeable battery [23-25], chemical sensor [26-30], photovoltaic cell [31-33], separation membranes [34-37], biomolecular immobilization matrices [38-40], corrosion devices and microwave absorption [41-45]. In addition, they can be used as conducting filler in insulating polymer matrices in preparation of electrically conducting composites. These composites offer potentials in electromagnetic interference shields, electronic packaging, display devices and electrodes [46-50].

Conductive polymers can be synthesized by electrochemical or chemical oxidation of corresponding monomers in various organic solvents and/or in aqueous media. The electrochemical process is more advantageous since film properties such as thickness and conductivity can be controlled by the synthesis parameters such as current density, substrate, pH, nature and concentration of electrolyte. Moreover, other advantages of electrochemical approach are doping is simultaneous, entrapment of molecules in conductive polymers, and ease of synthesis [51-58].

Zeolites are a large group of natural and synthetic, hydrated aluminosilicates (AS) of group I and group II elements, in particular, sodium, potassium, magnesium, calcium, strontium, and barium. They have three-dimensional network of $[AlO_4]^{5-}$ and $[SiO_4]^{4-}$ tetrahedrally linked to

each other by sharing all of the oxygen atoms. Zeolites form in nature as a result of the fusion of volcanic lava and ocean water millions of years ago, containing alkali and alkaline-earth hydrated aluminosilicates. However, nature requires 50 to 50,000 years to complete the reaction. There are over 45 varieties of natural zeolite minerals which have been identified and more than 150 zeolites have been synthesized. The most common of natural zeolites are analcime, chabazite, clinoptilolite, erionite, mordenite, and phillipsite while as for synthetic zeolites; the most common are zeolites A, X, Y, and ZSM-5 [59-65]. Synthetic zeolites have a wider range of properties and larger cavities than their natural counterparts. Moreover, the synthetics can, of course, be manufactured in a uniform, phase-pure state and it is possible to manufacture desirable zeolite structures which do not appear in nature [66,67].

Their crystalline framework is arranged in a unique interconnecting lattice structure. The general chemical formula of zeolite is $M_{x/n}$ $[(AlO_2)_x(SiO_2)_y]\bullet wH_2O$, where M is an alkali or alkaline earth cation, n is the valence of the cation, w is the number of water molecules per unit cell, x and y are the total number of tetrahedral per unit cell, and the ratio y/x usually has values of 1 to 5 [68-72]. In recent years, zeolites have attracted much attention due to their well-defined micro and nanopore sizes for molecular shape selectivity, large specific surface areas, intrinsic acidity, high (hydro)thermal, chemical stability, and wide range of commercial and technological applications such as molecular sieves, ion-exchangers, adsorbers, catalysts, detergent builders, cement (natural zeolites), agricultural use, and selective removal of heavy metal ions from sea water and industrial waste waters [73-81].

Composites are materials made from a mixture of a minimum of two components which, when combined, produce a material with significantly different physical or chemical properties which are superior to those of the individual materials. When the dispersed phase is in the nanometer scale, at least in one dimension, the hybrid is called a nanocomposite [82-87]. In nanocomposites incorporation of a few percent of nanofiller in matrix, often

remarkably enhanced physicochemical properties, which are rarely present in pure material or conventional composite. These improvements in the properties are the result of the nanometer scale dispersion of filler in the matrix [88-91]. In this respect, conductive polymers/zeolite (nano-)composites could be used as beneficial hybrid materials in wide range of commercial and technological applications such as sensors, cathodes of the cells, anticorrosive, membranes, and selective removal of heavy metal ions from sea water and industrial waste waters. However, these materials were sub-exploited and there was only a few researches conducted for the preparation and application of conductive polymers/zeolite hybrids.

There are numerous reviews are available around the synthesis, properties, and applications of zeolites and conductive polymers. However, to the best of our knowledge, the presented review is the first comprehensive article around the synthesis, materials properties, and applications of conductive polymers/zeolite (nano-)composites until March 2014.

2. Preparation methods of conductive polymers/zeolite (nano-)composites

The incorporation of the functional conductive polymer chains inside the cavities of zeolites improved their alignment and is expected to decelerate aging and to increase their electrical conductivity. Furthermore, the acidity of the zeolite surface ensures the excellent adhesion of the two materials, and a conductive polymer/zeolite system combines the fast electronic mobility of the polymer with the capability of the zeolite to accommodate exchangeable cations into its structure [93,100].

Conductive polymers/zeolite (nano-)composites can be prepared by four different routes: (i) the monomer is dissolved in a organic solvent and by diffusion processes is encapsulated into the cavities of zeolite, and then polymeric chains formed into cavities of zeolite by oxidation polymerization method [92- 94], (ii) the zeolite having oxidant ions, such as Fe(III) or Cu(II) is exposed to monomer and acid vapors, respectively [95,96], (iii) mechanical mixing of conductive polymer and zeolite powder [97-101], and (iv) *in situ* polymerization of

corresponding monomer in the presence of zeolite, which it is possible polymer formed within the zeolite channels and also outside of the cavities of zeolite [102,103]. Among the mentioned procedures for synthesis of conductive polymers/zeolite (nano-)composites, two specific methods (i and ii) are more attractive because of; polymeric chains can be synthesized into cavities of zeolite in the nanometer size domain and may be improved their electronic, mechanical, chemical, and optical properties due to the organization of the polymeric chains in the nanometer scale. All procedures to synthesis of conductive polymers/zeolite (nano-)composites, their materials properties, and applications are discussed in the following sections.

3. Polyaniline/zeolite (nano-)composites

Polyaniline (PANI), one of the most extensively investigated conducting polymers, has attracted a great deal of interest because of good electrical conductivity, environmental stability, easy synthesis, and controllability of its electronic and optical properties through variation of the degree of oxidation and protonation [104-106]. Three different types of basic PANI, *i.e.*, fully reduced leucoemeraldine (LEB) (x=0), half oxidized emeraldine (EB) (x=0.5), and fully oxidized pernigraniline (PAB) (x=1) are known (Scheme 1). An efficient and versatile method to control the polyaniline bulk properties such as electronic, mechanical, chemical, and optical is through the organization of the polymeric chains in the nanometer scale. In this respect, polymerization of aniline inside the cavities of porous inorganic hosts such as zeolite may be the efficient choice [107,108].

(Scheme 1)

Olad and Naseri [109] reported the synthesis of polyaniline/natural clinoptilolite (Clino) nanocomposites with various weight ratios (1, 3 and 5%, w/w) of clinoptilolite by *in situ*

polymerization of aniline in the presence of acidic clinoptilolite. It is proposed that the weakly polar aniline finds it more difficult to penetrate into the clinoptilolite channels than a polar anilinium cation. Aniline which exists as anilinium cation in strong acidic conditions of HCl (1M) solution can be exchanged by H^+ cations of acidic clinoptilolite [109]. They utilized FTIR spectroscopy, X-ray diffraction (XRD), scanning electron microscopy (SEM) and cyclic voltammetry (CV) techniques to confirm the incorporation of polyaniline in the clinoptilolite channels and formation of nanocomposites.

Moreover, they converted the synthesized green emeraldine nanocomposites to the blue emeraldine base form by deprotonation in an aqueous ammonia solution and investigated the anticorrosive performance of the synthesized nanocomposites coating on iron samples. They found that in acidic (HCl and H_2SO_4, 1M), and sodium chloride (3.5%, w/w) environments coating of iron samples with PANI/Clino nanocomposites resulted to enhanced corrosion protection effect in comparison to pure polyaniline coated samples. Comparative experiments revealed that PANI/Clino nanocomposite with 3% (w/w) clinoptilolite content had the best protective properties. It is demonstrated that the corrosion potential of PANI/Clino (3%, w/w) nanocomposite coated sample was more positively shifted than PANI/Clino nanocomposites with 1 and 5% (w/w) clinoptilolite content coated samples specially in sodium chloride (3.5%, w/w) solution.

Nascimento and Temperini [95] described the synthesis of polyaniline in the cavities of zeolites Y (ZY) and mordenite (MOR) having Cu(II) as oxidant agent. They utilized resonance Raman, UV–vis–NIR, FTIR and X-ray absorption near edge spectroscopy at the nitrogen *K* edge (N *K* XANES) techniques to analysis of PANI formed in the zeolite channels. For PANI-ZY composite was verified the presence of PANI chains outside the cavities, since it was observed lower crystallinity, higher organic content, and higher conductivity than other composites. The conductivity values observed for the inorganic hosts

before and after exposure to aniline and HCl vapors are shown in Table 1. A great increase (10^5 orders of magnitude) in the conductivity was observed for PANI-ZY, due to the presence of PANI chains outside the cavities of zeolite Y. Moreover, the amount of PANI by thermal analysis results was estimated as 7.5 wt%, and 29 wt% for PANI composites with MOR, and ZY materials, respectively. The higher amount of PANI observed for PANI-ZY composite means that there is PANI adsorbed outside the ZY porous, corroborating the XRD data. As they concluded, in the both composites the structure of PANI formed was different from the ‘‘free” polymer and the presence of Cu(II) ions leads to the formation of Phenosafranine-like rings. On the other hand, the presence of Cu(II) ions, associated to the zeolite structure leads to the formation of structures similar to the Phenosafranine (PSF units). The presence of these Phenazine-like rings in the structure of confined PANI chains can also contribute to the enhancement of the thermal stability observed for both composites [95].

(Table 1)

Chuapradit et al. [110] reported the preparation of polyaniline/zeolite LTA composites and investigated the electrical conductivity response of the prepared composites towards carbon monoxide (CO) in terms of dopant type, dopant concentration, zeolite LTA content, and zeolite pore size. For this purpose, they synthesized HCl and maleic acid (MA) doped polyaniline. The doped polymer powder was then dry mixed with three types of zeolite LTA (3A, 4A, and 5A) to produce polyaniline/zeolite LTA composites. They found that zeolite 4A reduces the electrical conductivity response but improves the sensitivity towards CO with increasing zeolite concentration up to 40% w/w. The polyaniline/zeolite 3A composite had a comparable sensitivity value relative to that of neat PANI. In addition, composites of 4A and 5A had greater sensitivity values over that of the neat PANI at the CO concentration range

between 16 and 1000 ppm. They concluded that the zeolite 5A was the most effective mesoporous material in promoting interaction between CO and polyaniline because of its largest pore size of 5 Å, relative to the zeolite 3A and 4A which have the pore sizes of 3 and 4 Å, respectively.

In another study, Densakulprasert et al. [111] synthesized PANI/zeolite composites and investigated ion exchange capacity of composites on electrical conductivity response to carbon monoxide (CO). For this purpose, zeolite Y, and 13X containing cation Cu^{2+} dry mixed with synthesized maleic acid (MA) doped polyaniline and compressed to form polyaniline/zeolite pellet composites. They found that with an addition of 13X zeolite to pristine polyaniline, the electrical conductivity sensitivity to CO/N_2 gas increases with zeolite content. For the effect of zeolite type, the higher electrical conductivity sensitivity was obtained with the 13X zeolite. Y zeolite and 13X zeolite have comparable pore sizes but the 13X zeolite has a greater pore free volume and a more favourable location distribution of the Cu^{2+} ions within the pore. They concluded that the temporal response time increased with the amount of zeolite in the composites but it was inversely related to the amount of ion exchange capacity. The mechanism proposed by Densakulprasert et al. for the CO-PANI interaction is shown in Scheme 2.

(Scheme 2)

Shyaa et al. [112] synthesized polyaniline/zeolite nanocomposite by the polymerization of anilinium cation in and out-side of zeolite channels. The products were characterized by UV–visible, FTIR, ^1H NMR, XRD, SEM and TGA techniques. The SEM images of the pure PANI (A) and PANI/zeolite nanocomposite (B) are shown in Figure 1. SEM images showed that the diameter of the PANI/zeolite nanocomposite was between 300 and 600 nm. Thermal

property study by TGA showed that the extent of decomposition of PANI/zeolite nanocomposite (560 °C) was less than that of pure polyaniline (490 °C), which can be explained by the strong interaction between PANI and zeolite. The synthesized polyaniline/zeolite nanocomposite was used for removal of chromium(VI) from aqueous solution. They found that the capacity of chromium adsorption on PANI/zeolite nanocomposite increased with initial metal concentration, the metal ion adsorption on surfactant was well represented by the Freundlich isotherm. Moreover, they studied the effect of pH on the chromium adsorption process on PANI/zeolite nanocomposite, over the pH range 2–9, using 0.2 g PANI/zeolite nanocomposite and 50 ppm chromium solution. The obtained results are shown in Figure 2. It is clear that the maximum adsorption of Cr(VI) occurred at pH 2–6, and decreased at higher pH values.

(Figure 1)

(Figure 2)

Ma et al. [113] reported the synthesis of PANI/β-zeolite and PANI/FUYB-zeolite nanocomposites *via* oxidative polymerization of absorbed aniline monomers in the channels of corresponding zeolite type in hydrochloride solution. The synthesized nanocomposites were coated on the interdigital electrodes of carbon with casting method and investigated gas sensitivity of the casted films to a series of chemical vapours such as trimethylamine, triethylamine, ammonia, and water. Gas sensitivity of the composite films to trimethylamine strongly depended on the type of zeolite added. They found that for the system containing β-zeolite, the gas sensitivity to trimethylamine decreased significantly compared with that of polyaniline film and for FUYB-zeolite, it was enhanced remarkably. Moreover, the results

indicated that, in comparison with the polyaniline film prepared by normal *in situ* polymerization, not only the morphology of polyaniline composites was clearly different, but also the heat stability of polyaniline film was improved significantly by adding zeolite.

Malkaj et al. [97] prepared solid state electrodes sensitive to pH constructed from polyaniline/zeolite and polypyrrole/zeolite conductive blends. For this purpose, they polymerized aniline and pyrrole monomers in the presence of predetermined amount of zeolite at room temperature in 0.2M HCl aqueous solution. Afterwards, PANI/zeolite and PPy/zeolite blends disc-shaped specimens 13 mm in diameter and 1.5 mm thick were made in an infrared press with 22.7 and 22 w/w content in zeolite, respectively. They investigated that these sensors were stable in aqueous electrolyte solutions of low pH value at temperatures up to 45 °C with response time in seconds. The electromotive force E *versus* the pH values for the PANI/zeolite-Pt and PPy/zeolite-Pt cells are shown in Figure 3. At 25 °C, sensor sensitivity was -310 ± 40 mV/pH and -1300 ± 100 mV/pH for polyaniline and polypyrrole blends, respectively.

(Figure 3)

More recently, Jiang et al. [114] studied the electrorheology (ER) of suspensions based on polystyrene/polyaniline (PSt/PANI) core/shell structured microspheres and those based on disk-like zeolite particles at different electric fields and particle volume fractions. For this purpose, monodisperse PSt core particles were firstly synthesized *via* a dispersion polymerization method, then the fine coating for which by conducting PANI was realized by a swelling–releasing process in an aqueous suspension of the particles by adding aniline monomer. The synthesized PSt/PANI microspheres were subsequently mixed with NaY type zeolite in silicone oil, with nominal particle volume fraction ranging from 5 to 39 vol%. Both

types of ER fluids showed abrupt shear thickening under high electric fields and low shear rates, as well as shear thinning when the shear rate increased. A normalized method that considers the effects of electric field strength, shear rate and particle volume fraction was proposed to compare the rheological curves of the two ER fluids.

Ivan et al. [115] synthesized polyaniline/zeolite 5A composite and investigated its capability for recovery or removal of cobalt ions from waste water by ultrafiltration. The membrane material was obtained by *in situ* oxidative polymerization of aniline in synthetic zeolite matrix. Figure 4 shows the SEM images of zeolite 5A (a, b), and polyaniline/zeolite 5A composite (c, d) at different magnifications. They tested the retention capability of zeolite 5A, polyaniline (PANI), and PANI/zeolite 5A composite for cobalt ions from synthetic aqueous solutions (10^{-4}-10^{-6} M), and the obtained results are summarized in Table 2.

(Figure 4)

(Table 2)

Milojevic-Rakic et al. [116] synthesized polyaniline/ZMS-5 zeolite composites and evaluated their adsorbents of the organic herbicide glyphosate [*N*-(phosphonomethyl)glycine] in aqueous solution. The adsorption isotherms of glyphosate on studied materials were best fitted by Freundlich and Langmuir–Freundlich models. The highest adsorption of glyphosate among all investigated PANI, pure ZSM-5, and PANI/ZSM-5 samples, exhibited the deprotonated granular PANI which was synthesized in sulfuric acid medium (98.5 mg/g). High adsorption capacity also showed the deprotonated PANI/ZSM-5 composite with ~50% of zeolite (61.9 mg/g), and the protonated nanostructured PANI (59.9 mg/g), both materials prepared in water without added acid.

Safidine et al. [117] reported synthesis of conducting polyaniline/zeolite (PANI-HY) composites by two different methods and investigated their capability for a carbon dioxide (CO_2) gas sensor. The first method utilized *in situ* polymerization of aniline with ammonium peroxydisulfate as an oxidizer in an aqueous medium with addition of zeolite type HY-free acids. The second method involved the dispersion of various fractions of HY (5, 10, 15, 20 and 50 wt %) in a PANI-HCl matrix by physical mixing. They concluded that, the PANI-HY composite exhibited a lower conductivity by 7.74×10^{-3} to 10^{-2} S cm^{-1} when compared with PANI doped by HCl. In fact, the conductivity of the synthesized composites increased with exposure to CO_2; this behavior was well-observed and described as an interaction between PANI and acidic CO_2 molecules. Moreover, the synthesized PANI-HY composite showed rapid response time towards CO_2.

4. Polypyrrole/zeolite (nano-)composites

Polypyrrole (PPy) has been the subject of considerable recent interest because of its unique properties such as good electrical conductivity, easy synthesis, thermal and environmental stability, and numerous potential applications [118-122]. Scheme 3 shows the synthesis of PPy *via* chemical oxidation polymerization using $CuCl_2$ as an oxidant and description of redox reaction of polypyrrole. In recent decades, several attempts have been made to control and improve the physical, structural, optic and electronic properties of conductive polymers. Encapsulation of conductive polymers in heterogeneous hosts such as zeolites is an efficient and versatile method to control and improve the aforementioned properties of these polymers [123-129].

(Scheme 3)

Cho et al. [130] applied surfactant bilayers adsorbed on TS-1 zeolite as templates to produce colloidal nanocomposites with a polypyrrole shell. For this purpose, the TS-1 zeolite particles were dispersed in water at pH = 8, followed by adding cetylpyridinium chloride (CPC). The resulting mixture was allowed to equilibrate at 25 °C for 1 day. After 24 hours of equilibration, various amounts of pyrrole were added to the solution which was further equilibrated for another 24 hours. The same experiment was carried out without using CPC to observe the adsorption of pyrrole on the TS-1 nanoparticles. Templated pyrrole polymerization was slowly initiated by adding an equimolar amount of ferric trichloride ($FeCl_3$), which is dissolved in 0.5 mL of water, to the loaded pyrrole. A schematic of the synthesis procedures for preparation of core-shell nanocomposites utilized by Cho et al. is shown in Figure 5. It was found that the adsorbed surfactant (CPC) plays a critical role for attaining both the colloidal stability of the nanocomposites and an enhanced conductivity of the PPy sheath on the TS-1 core. The observed contact conductivity of the nanocomposites was 5 S cm^{-1} for a sample with 8 wt% of PPy incorporation, while bulk PPy powder had a contact conductivity of 0.03 S cm^{-1}. The high contact conductivity was originated from the enhanced molecular order of polymer chains that were grown in the nanoscopically confined environment. Moreover, transmission electron microscopy (TEM) images showed that the formation of ultrathin PPy films (10-30 nm) on nanosized particles (100 nm) can be accomplished on a preparative scale using self-assembled arrays (SAAs) of CPC on TS-1 zeolite nanoparticles as a template.

(Figure 5)

Rashidzadeh et al. [93] reported the synthesis and characterization of polypyrrole/clinoptilolite nanocomposite by *in situ* surface polymerization of pyrrole

monomer using Fe^{3+} as oxidant, incorporated on the inner and outer surface of clinoptilolite nanoparticles. Elemental analysis showed the loading/incorporation of 9.18 wt% polypyrrole in the clinoptilolite structure. They found that the electrical conductivity of polypyrrole/clinoptilolite nanocomposite pellets (45.57 S cm^{-1}) was higher than that of similar pure polypyrrole pellets (34.72 S cm^{-1}), synthesized through the chemical oxidation polymerization method using Fe^{3+} as oxidant without the presence of clinoptilolite nanoparticles. This is may be originates from the increasing of chain alignment of PPy in nanocomposite structure. Moreover, the scanning electron microscopy (SEM) images showed that the structural order and chain alignments of polypyrrole were improved by deposition on the surface of clinoptilolite nanoparticles (Figure 6). The electroactivity of the polypyrrole/clinoptilolite nanocomposite was confirmed under cyclic voltammetric conditions, as shown in Figure 7. It is believed that the observed electroactivity reflects the redox activity of the included PPy on the surface and in the pores of clinoptilolite nanoparticles. This electroactivity was also related to the deprotonation/protonation of PPy chains [93].

(Figure 6)

(Figure 7)

Uehara et al. [131] synthesized encapsulated polypyrrole in two kinds of zeolite Y (NaY and USY) with various concentrations of Cu^{II} ions. For this purpose, firstly sodium and proton ions in zeolites were ion-exchanged with Cu^{II} ions at 50 °C for 48 hours, using various concentrations (1.0, 0.1, 0.01, and 0.001) of Cu^{II} ions. The ion-exchanged zeolites and ion-unexchanged zeolites were calcined, and then pyrrole molecules were loaded by means of a

gas diffusion process for 2 hours. Afterwards, the samples were evacuated for 2 hours to remove excess pyrrole molecules adsorbed on the surface of the zeolites. Calcination and encapsulation were continuously carried out in the closed system without exposing the zeolites to the air. They found that the progress of polymerization depended on the Cu^{II} content, *i.e.* pyrrole was encapsulated as polypyrrole in both NaY and USY zeolites with a high concentration of Cu^{II} ions, and predominantly as pyrrole oligomer and/or monomer in those with a low concentration of Cu^{II} ions. Furthermore, electron paramagnetic resonance (EPR) spectra revealed that NaY with a high concentration of Cu^{II} ions was active for the formation of bipolaron polypyrrole in the framework, whereas USY with a high concentration of Cu^{II} ions was not. Thermal property study (TG–DTA) showed that thermal stability of polypyrrole in pyrrole/Cu-USY was higher than that in pyrrole/Cu-NaY. They concluded that the electrical conductivities of NaY and USY were presumed to increase with polypyrrole loading in the zeolite channels. Figure 8 shows the frequency dependences of the electrical conductivities of NaY and USY before and after loading of polypyrrole. Significant differences of electrical conductivities before and after pyrrole loading were observed in the high frequency region, although the electrical conductivities were low. The low electrical conductivities were interpreted to be due to the fact that the electrodes on the powder-compacted disk did not come into complete contact with polypyrrole prepared in the zeolite channels [131]. The electrical conductivity of pyrrole/1.0Cu-NaY was about four times higher than that of pyrrole/1.0Cu-USY in the high frequency region.

(Figure 8)

Polypyrrole/zeolite (nano-)composite can be prepared by electrochemical polymerization method. Using electrochemical polymerization Trueba et al. [132] synthesized polypyrrole

nanowires in the nanochannels of a proton-modified natural zeolite clinoptilolite (HNZ) and Y zeolite in acid form (HY). They found that the generation of PPy with electrochemical activity was favored in a strongly acidic nanoscaled environment, in comparison with the polymer synthesized in the hosts without previous proton modification. It was proposed that the reduction/oxidation responses are a consequence of the polymer protonation/deprotonation where the H^+ ions possibly act as charge transfer promoters. Cyclic voltammetry study of the synthesized PPy-HNZ and PPy-HY showed the well defined redox signals of PPy included in HNZ, compared to the HY, suggest that the polymeric units were held more tightly to the channels walls due to its complex framework. They concluded that the one electron oxidation process did not depend on first order monomer concentration but lower (0.38) for PPy growth in HNZ, which was related to the spatial restriction of the host.

In another study, Nakayama et al. [133] synthesized PPy-Y zeolite composite by electrochemical polymerization of pyrrole in the presence of Y zeolite. It was demonstrated from the XRD pattern that the PPy in the composite was located within the channels of Y-zeolite, in which the cationic PPy was in combination with the negative surface of Y-zeolite. The electron spin resonance (ESR) spectra of the PPy/Y-zeolite composite and pure PPy films deposited on Pt rod electrode are shown in Figure 9. Electron spin resonance spectrum of the PPy/Y-zeolite composite film exhibited the resonance signal characteristic of conducting polymer in a partially oxidized (polaron) form. The optical intensity of this spectrum was considerably smaller than that of pure PPy, suggesting that a certain portion of PPy in the composite was stabilized by the formation of bipolarons (diamagnetic) [133]. They concluded that the PPy incorporated in the zeolite channels was found to be reduced to the neutral form and the charge to be balanced by the incorporation of electrolyte cations.

(Figure 9)

Conductive polypyrrole/zeolite (nano-)composites can be applied as a sensitive sensors to detection of various chemical vapors and biological samples. Polypyrrole/zeolite (nano-)composites have the advantage of fast electronic mobility of polypyrrole and the capability of zeolite to incorporate cations into its structure [97,127]. Wannatong and Sirivat [134] investigated the sensing application of chemically synthesized polypyrrole and PPy composites with 3A zeolite (3A), and polyamide 6 (PA): *i.e.* PPy_3A50 pellet, PA20_PPy13_3A50 film, and PA20_PPy13_3A50 electrospun fiber bundle, for four chemical vapors that are the common components of lacquer: acetone, methyl ethyl ketone (MEK), methanol, and toluene. The electrical sensitivity of the four sensing materials towards vapor of acetone, MEK, methanol, and toluene, at 3 vol% in N_2 are shown in Figure 10. As shown in Figure 10 in this condition PPy_3A50 pellet and PA20_PPy13_3A50 film exhibited the highest selectivity towards methanol relative to other three chemical vapors, whereas the PA20_PPy13_3A50 electrospun fiber bundle was relatively insensitive to all of the chemical vapors. For the insensitive PA20_PPy13_3A50 fiber, the conducting PPy particles are too far from each other; this leads to not only poor specific electrical conductivity of the material, but also the low electrical sensitivity from the swelling effect.

(Figure 10)

Wang et al. [135] reported the synthesis and humidity-sensing properties of encapsulated nickel oxide (NiO) doped polypyrrole in mesoporous silica SBA-15. The surface morphology of the synthesized SBA-15 and NiO–PPy/SBA-15 were observed by scanning electron microscopy (SEM). For the neat SBA-15, the morphology consisted of some short rods. The diameter of these rods was about 300 nm (Figure 11a). However, when the PPy was

encapsulated into SBA-15, it obtained the morphology of a bunch of rods. It is clear from Figure 11b, this morphology was similar to the morphology of pure SBA-15. These results demonstrated indirectly the successful encapsulation of NiO–PPy into the channels of SBA-15. They investigated the sensitivity mechanism by direct-current (dc) and alternating-current (ac) analysis. In direct-current (dc) analysis the operation voltage was 1 V, and the current variations at low-humidity (Figure 12a) and high-humidity (Figure 12b) conditions are shown in Figure 12. In low-humidity environments, the current decreased linearly with increasing time. This indicated that only one type of carrier dominated the conduction in low-humidity environments. They suggested that this carrier was the electron. When the humidity became high, another peak was obtained on the curve (Figure 12b). The peak became higher when the humidity increased. This phenomenon indicated that another kind of carrier took part in conduction and its function strengthened with increasing humidity. They concluded that the principal conductive particle in high humidity was the ion. The transmission speed of the ion was lower than that of the electron [135].

(Figure 11)

(Figure 12)

Olad et al. [136] synthesized polypyrrole/clinoptilolite (PPy/CL) nanocomposite and investigated its efficiency for removal of Ni(II) from aqueous solutions in batch experiments. The effect of various factors such as solution pH, contact time, and concentration of Ni(II) solution on the removal efficiency were investigated. The optimum conditions for high removal efficiency included adjustment of solution pH value to 4, using nanocomposite for a time period of about 24 hours. The effects of contact time, and pH on the removal efficiency

of Ni(II) are shown in Figures 13 and 14, respectively. They concluded that, Freundlich isotherm has a better correspondence with the experimental findings rather than with Langmuir and the adsorption mechanism of nanocomposite is defined by both chelating and ion exchange.

(Figures 13)

(Figures 14)

Javadian et al. [137] synthesized polypyrrole/thiol-functionalized zeolite Beta/MCM-41 type mesoporous silica nanocomposite (PPy/SH-Beta/MCM-41), and investigated its capability for adsorption of Hg^{2+} from aqueous solution and industrial waste water. For this purpose, zeolite Beta/MCM-41 was modified by 3-mercaptopropyltrimethoxysilane (MPTMS), and then PPy/SH-Beta/MCM-41 nanocomposite was prepared by *in situ* oxidative polymerization of pyrrole monomers in the presence of SH-Beta/MCM-41. The calculated thermodynamic parameters (ΔH, ΔS, and ΔG) revealed that the adsorption of mercury ions onto PPy/SH-Beta/MCM-41 was an endothermic and spontaneous process. It was found that temperature has a positive effect on the removal efficiency and that PPy/SH-Beta/MCM-41 was potentially able to remove mercury ions from aqueous solutions at even high concentrations (400 mg L^{-1}). The effect of temperature on removal efficiency of mercury ions is shown in Figure 15. As they concluded, the recovery of Hg^{2+} from the PPy/SH-Beta/MCM-41 adsorbent was found to be more than 90% using 0.5 M H_2SO_4, and the ability of the absorbent to be reused for removal of Hg^{2+} was investigated. The results obtained for reusing the PPy/SH-Beta/MCM-41 after desorption is shown in Figure 16.

(Figure 15)

(Figure 16)

5. Polythiophene/zeolite (nano-)composites

Electrically conducting polymers have been widely studied over the past few decades due to their unique semiconducting and optoelectronic properties. In particular, π-conjugated polythiophene (PTh) stands out as one of the most promising members of the conjugated polymer family because of its excellent environmental and thermal stability, mechanical strength, magnetic, and optical properties, as well as its wide range of applications [138-145]. The generally accepted mechanism for the oxidative polymerization of thiophene involves the formation of radical cations. The oxidative polymerization of thiophene using $FeCl_3$ as an oxidant is shown in Scheme 4 [14,146].

(Scheme 4)

In recent decades, there has been much attention paid to the development of new organic/inorganic (nano-)composite materials for both optical and electronic applications. Among the wide range of organic/inorganic hybrid materials that may be suitable for the aforementioned applications, the (nano-)composites of conjugated polymers such as polythiophene (PTh) and its derivatives with zeolites are of particular interest. Zeolites can be incorporated into polythiophene to produce conducting (nano-)composites with improved physicochemical properties. Moreover, polythiophene may be polymerized inside the cavities of zeolite to produce PTh/zeolite (nano-)composite with controlled structure and properties [147-150].

Číka et al. [151] reported the synthesis of polythiophene/ZSM-5 photocatalyst system by *in situ* oxidative polymerization of thiophene with $FeCl_3$ in the suspension of Na-ZSM-5 zeolite. They investigated that the synthesized polythiophene absorbs radiation in the visible range of the electromagnetic spectrum and by illumination with visible light generates reactive oxygen species (ROS) in water medium. Moreover, during illumination reactive hydroxyl radical was detected by the spin trapping electron paramagnetic resonance (EPR) method. To examine the efficiency of the synthesized polythiophene/ZSM-5 photocatalyst system they tested it on the killing of *Gram*-positive bacteria Staphylococcus aureus (S. *aureus*) and *Gram*-negative bacteria Escherichia coli (E. *coli*). As shown in Figures 17 and 18 the number of living cells of both bacterial (G^+ bacteria S. *aureus* and G^- bacteria E. *coli*) species decreased in dependence on the amount of photocatalyst when treated with visible light (texp = 16 hours). However, it is clear from Figures 17 and 18, that, E. *coli* proved to be more sensitive then S. *Aureus*. Moreover, they concluded that the concentration of $^{\bullet}OH$ radicals, generated by irradiation with visible light, was able to decrease the number of surviving cell from 65% to 50%. Thus the synthesized polythiophene/ZSM-5 photocatalyst system may be applied in the protection of biologically contaminated environment.

(Figure 17)

(Figure 18)

Arvand et al. [152] developed a conductive polythiophene composite based on polythiophene/Y-zeolite *via* chemical oxidative polymerization of thiophene (Th) in the presence of a dispersion of Y-zeolite (powder) in chloroform solvent using anhydrous $FeCl_3$ as oxidant and investigated its response towards sulfide ions. As shown in Figure 19 SEM

and TEM images revealed formation of composite particles with average diameter in the range of 0.3–0.35 μm. The TEM image reveals a "raspberry" morphology where the zeolite particles were "glued" with the chains of PTh. Moreover, the flakes such as nature of PTh changed and distinctly shaped particles were formed, resulting in some improvement in the compactness of the polymer as well as in the decelerate aging and to increase their electrical conductivity.

They investigated that the synthesized PTh/Y-zeolite-$FeCl_3$ composite had a significantly high DC conductivity value (10^{-2} S cm^{-1}) compared to other PTh based systems. They suggested that appearance of high conductivity in PTh/Y-zeolite composite is a unique feature of this polymerization system. They applied the synthesized PTh/Y-zeolite composite as ion-selective electrodes (ISE) for the direct determination of sulfide ion in solution. As shown in Figure 20, among different anions, sulfide ion gives a better characteristic response. The selective electrode exhibited linear response to the activity of S^{2-} ions within the concentration range of 1×10^{-7} to 1×10^{-4} M with a Nernstian slope of 29.2±0.7 mV per decade (n=5). Proposed mechanism by Arvand et al. for the response mechanism of the sulfide ion-selective electrode based on PTh/Y-zeolite composite is shown in Scheme 5. Moreover, they concluded that the prepared electrode response was stable in relatively high temperatures. The electrode was successfully applied for the determination of S^{2-} content in aqueous solution with arrangement pH.

(Figure 19)

(Figure 20)

(Scheme 5)

Ballav and Biswas [153] reported the synthesis of conductive polythiophene/13X-zeolite composite by chemical oxidative polymerization of thiophene (Th) in the presence of a dispersion of 13X-zeolite (powder) in chloroform ($CHCl_3$) solvent using anhydrous ferric chloride ($FeCl_3$) as oxidant. DC conductivity value of the synthesized PTh/13X-zeolite composite was in the order of 10^{-2} S cm^{-1}, which was indeed high compared to that of PTh, produced under identical conditions as above without the presence of 13X-zeolite. The SEM images of 13X-zeolite (Figure 21a) and PTh/13X-zeolite composite (Figure 21b) are shown in Figure 21. In general, the SEM image of 13X-zeolite showed the presence of small nearly globular particles with irregular sizes (1.5–3.0 μm). In contrast, SEM image of PTh/13X-zeolite composite indicated the formation of lumpy agglomerates of non-uniform sizes (average diameter varied from 5.0 to 10.0 μm). They suggested that such morphology possibly resulted from cementation of the PTh moieties with 13X-zeolite particles. They concluded that, thermogravimetric stability studies revealed the overall thermal stability trend as follows: 13X > PTh-13X > PTh. The total weight loss up to 800 °C temperature suffered by pure 13X, PTh/13X and PTh homopolymers were 20, 65 and 100%, respectively [152].

(Figure 21)

McCann et al. [154] reported the polymerization of pyrrole and thiophene monomers into the copper-exchanged mordenite host. The synthesized composites were characterized using EPR and UV-vis absorption spectroscopy. The electron paramagnetic resonance (EPR) spectra showed a decrease in the intensity of the Cu^{2+} signal and the appearance of a radical signal due to the formation of oxidatively coupled oligomeric and/or polymeric chains in the zeolite host. Moreover, they investigated that the reaction ceases when *ca.* 50% of the copper has

reacted and differences in the form of the residual Cu^{2+} signal between the thiophene and pyrrole reactions suggest a greater degree of penetration of the reaction into the zeolite host for pyrrole. The EPR signal intensities revealed that the average length of the polymer chain that was associated with each radical centre was 15-20 and 5-7 monomer units for pyrrole and thiophene, respectively. As shown in Table 3 the widths of the EPR signals suggested that these were at least partly due to small oligomers. The results, displayed in Table 3, confirm that polymer growth was diffusion limited on zeolite samples and also indicated that shorter polymer chains were formed within HM.

(Table 3)

Thuwachaowsoan et al. [99] described the synthesis of poly(3-thiopheneacetic acid), (P3TAA), composites with zeolites L (L), mordenite (MOR), and beta (BEA) through random dry mixing. The fabricated composites were applied as gas sensor toward H_2, and the electrical conductivity response toward H_2 was investigated for the effects of zeolite contents, zeolite type, cation type, and cation concentration. They found that the negative electrical conductivity response and sensitivity generally occurred when exposed to H_2 relative to N_2, due to a weaker interaction between H_2 and the polaron or the bipolaron species compared to the interaction between N_2 and active sites of the perchloric acid doped P3TAA. The proposed mechanism by Thuwachaowsoan et al. for the H_2-P3TAA interaction is shown in Scheme 6. The highest electrical conductivity sensitivity value was obtained with 20% (v/v) MOR. However, the reduction of sensitivity values occurred with increasing MOR zeolite concentration from 20 to 50% (v/v); this arises from the diminishing active sites available for the interaction between H_2 and the polaron or the bipolaron species. On the other hand, for the composites with 20% (v/v) L, MOR, and BEA, the electrical conductivity sensitivity

increased with decreasing Al content because of a lesser interaction between H_2 and the zeolite, and consequently a greater interaction between H_2 and the active sites on the P3TAA chain. For the effect of cation type, the higher electronegativity and smaller ionic radius of Li^+ loaded into the MOR zeolite framework causes the lowering of electrical conductivity sensitivity than the composites loaded with Na^+ and K^+. They concluded that for composites with zeolite L loaded with Na^+ at 0, 15, 20, 30 and 50 mol%, the electrical conductivity sensitivity increased with increasing Na^+ content up to 30 mol% and decreases beyond that [99].

(Scheme 6)

6. Other conductive polymers/zeolite (nano-)composites

In previous sections the synthesis methods, some properties, and applications of PANI, PPy and PTh (nano-)composites with synthetic or natural zeolites have been discussed. However, other conducting polymers such as polyfuran, poly(*N*-vinylcarbazole), poly(*p*-phenylene vinylene), and poly(*p*-phenylene) have been applied for preparation of conductive polymers/zeolite (nano-)composites. The synthesis methods, some properties and applications of these (nano-)composites are discussed in the following.

More recently, Kamonsawa et al. [155] reported the synthesis of H_2SO_4 doped poly(*para*-phenylene vinylene) (dPPV)/zeolite Y-based composite and investigated its sensitive and selective responses toward ketone vapors. The morphology of the synthesized materials by Kamonsawa et al. is shown in Figure 22. The dPPV particles are quite irregular in shape and size, as shown in Figure 22a. On the other hand, the zeolite Y appears to possess nearly uniform sizes and shapes, as shown in Figure 22b. However, a nearly uniform dispersion of dPPV particles within the NH_4^+Y matrix can be observed in Figures 22c and 22d. They

studied the effect of cation type (Na^+, NH_4^+, and H^+), cation concentration, and ketone vapor type on the electrical conductivity response toward ketone vapors of dPPV/zeolite Y composites. They found that the sensitivities of the synthesized composites increase linearly with increasing surface area and decreasing cationic radius of the cation in zeolite Y. The highest sensitivity was obtained with the dPPV_[90] NH_4^+Y when exposed to acetone, whereas in 4-methylpentan-2-one (MIBK) showed the lowest sensitivity. The sensitivity values of dPPV, dPPV_[90]HY, dPPV_[90]NaY, and dPPV_[90] NH_4^+ Y, when exposed to acetone, methyl ethyl ketone (MEK), and 4-methylpentan-2-one (MIBK) is shown in Figure 23. Moreover, the interactions between the ketone molecules and the composites were investigated though the FTIR spectroscopy.

(Figure 22)

(Figure 23)

Among the conjugated polymers, polyfuran (PFu) has received relatively less attention than polypyrrole, polythiophene, and polyaniline, because of the high moisture sensitivity, difficulty of synthesis as the monomer has high oxidation potential, and low electrical conductivity owing to the short conjugated segment in its polymeric chains [156-158]. However, polyfuran can be used as a humidity sensor, and acts as an optoelectronic device since its color changes from yellow-brown to black-brown upon doping [159-161]. Polyfuran can be synthesized by both chemical, and electrochemical methods in various organic solvents and/or in aqueous media. The structure of this polymer has been reported as planar (Scheme 7).

(Scheme 7)

The incorporation of zeolites as inorganic fillers into polyfuran matrixe or *in situ* polymerization of furan inside the cavities of zeolite may be bring a new class of organic-inorganic (nano-)composite materials with improved physicochemical properties for various practical and technological applications. Şena et al. [162] reported the preparation of polyfuran composites with LTA type (3A, 4A, 5A) zeolites, via chemical oxidative polymerization of furan in the presence of a dispersion of zeolites (powder) in acetonitrile solvent using anhydrous $FeCl_3$ as oxidant at an ambient temperature. They utilized Fourier transform infrared spectroscopic (FTIR) analysis to investigation of adsorption properties of synthesized composites for benzoyl chloride. FTIR results showed that the composites of 3A zeolite with the smallest pore size did not indicate absorption for benzoyl chloride due to surface structural of OH groups. The electrical conductivity value of PFu synthesized using $FeCl_3$ was found to be 3.99×10^{-5} S cm^{-1}, while the conductivity of PFu was decreased a bit after preparing its zeolite composites. Among PFu/LTA composites the highest conductivity value (3.34×10^{-5} S cm^{-1}) was observed for 3A/PFu composite. A conductivity value of 4A/PFu and 5A/PFu composites was found to be 9.87×10^{-6} and 8.47×10^{-6} S cm^{-1}, respectively. They concluded that due to pore size of nanometer scale in zeolite, it was a promising material for conducting polymers.

In another study, Sardar et al. [163] reported the synthesis of highly conductive polyfuran/13X zeolite/polyaniline composite *via in situ* chemical oxidative polymerization of furan monomer with anhydrous $FeCl_3$ in the presence of 13X zeolite, followed by the oxidative copolymerization of aniline with ammonium peroxydisulfate (APS) in the presence of an aqueous dispersion of preformed PFu/13X composite. Some typical data on the polymerization and synthesized composite by Sardar et al. are summarized in Tables 4 and 5.

They performed thermogravimetric analysis (TGA) and differential thermal analysis (DTA) for investigation of thermal properties of the synthesized materials. Characteristic TGA curves of the 13X zeolite, PFu/13X (loading of PFu is 80%), PANI-PFu/13X (loading of PFu is 80% and PANI is 65%), and PFu are shown in Figure 24. As shown in Figure 24 the thermal stability order was found to be 13X > PFu/13X > PANI-PFu/13X > PFu. Moreover, the dc conductivity of PFu/13X, and PANI-PFu/13X was found 10^{-8} and 1 S cm^{-1}, respectively.

(Table 4)

(Table 5)

(Figure 24)

Phumman et al. [164] reported the fabrication of poly(*p*-phenylene)/ZSM-5 zeolite composites, and investigated their responses towards ammonia. For this purpose, they synthesized poly(*p*-phenylene) (PPP) *via* oxidative polymerization of benzene in the presence of anhydrous aluminum chloride, and anhydrous cupric chloride at a mole ratio of 8:2:1, followed doping by $FeCl_3$. The poly(*p*-phenylene)/ZSM-5 zeolite composites were prepared by dry mixing of $FeCl_3$-doped poly(*p*-phenylene), and ZSM-5 zeolite at various zeolite amounts: 10%, 20% 30% and 40% v/v, in order to investigate the effect of zeolite content. Moreover, the effect of cation type (NH_4^+, Na^+, K^+, and H^+) in the electrical conductivity sensitivity towards ammonia were investigated. It was found that the electrical conductivity sensitivity of the composites with different cations in the zeolite can be arranged in this order: K^+ < no zeolite < Na^+ < NH_4^+ < H^+. The variation in electrical sensitivity with cation type can

be described in terms of the acid-base interaction, the zeolite pore size, and surface area. They concluded that the PPP/Zeolite composite with H^+ possesses the highest electrical sensitivity of −0.36 since H^+ has the highest acidity, the highest pore volume and surface area, which combine to induce a more favorable NH_3 adsorption and interaction with the conductive polymer.

7. Summary and conclusion

Conductive polymers can be applied in different areas such as chemistry, physics, electronics, optics, materials, and biomedical sciences. These applications reflect their characteristic properties, such as their conductivity, good thermal and environmental stability, relatively easy preparation, their change in electrical conductivity or color when exposed to acidic, basic and some neutral vapors or liquids, very high capacitance values, etc. Moreover, in recent decades, there has been growing interest in the development of organic-inorganic hybrid materials in order to obtain new kind of materials with synergetic or complementary behavior for various practical and technological applications. In this respect, conductive polymers/zeolite (nano-)composites may be the efficient choice as beneficial hybrid materials in wide range of commercial and technological applications such as sensors, cathodes of the cells, anticorrosive, membranes, removal of toxic heavy metals from sea water and waste waters. However, these materials were sub-exploited and there was only a few researches conducted around the preparation and applications of conductive polymers/zeolite hybrids.

This review has presented the developments in preparation, materials properties, and applications of conductive polymers/zeolite (nano-)composites until March 2014. It is well established that zeolites are one of the most promising host materials for incorporation of conductive polymer network owing to their highly ordered pore systems, channels, and cages of different dimensions and shapes and the surface with negatively charge-balanced with exchangeable cations. Moreover, the intercalation of a conductive polymer into a porous and

leafy material, like zeolite, protects the former from degradation, slowing down its aging rate. In comparison with corresponding pure polymers the conductive polymers/zeolite (nano-)composites exhibit fast reversible electrical conductivity responses when exposed to gases or vapors at room temperature. Thus, these hybrids have good perspective for development of sensors. Furthermore, as a sensing material, zeolites are very advantageous: chemical resistance and high thermal stability. When the conductive polymers/zeolite (nano-)composites applied as a cathodes for the cells, the advantage of zeolite compared to other materials is that it ensures great effective surface, on which cations can be arranged by adsorption, intercalation or cation exchange reaction. This results in the minimization of the cell volume, minimizing the internal resistance, and the full exploitation of the electrode.

In conclusion, some good results were obtained in the applications of conductive polymers/zeolite (nano-)composites in the various practical and technological applications. Thus, it would be expected that conductive polymers/zeolite (nano-)composites could further applications in the coming decades because of their unique physicochemical properties.

Acknowledgment

I wish to express my gratitude to the Research Center for Pharmaceutical Nanotechnology, Tabriz University of Medical Sciences for partial financial supports.

References

[1] S. Yuan, Q. Tang, B. He and P. Yang, *J. Power Sources.,* 2014, **254**, 98-105.

[2] S. Ni, H. Li, S. Li, J. Zhu, J. Tan, X. Sun, C. P. Chen, G. He, D. Wu, K. C. Lee, C. C. Lo, A. Lien, J. Lu and Y. Su, *J. Mater. Chem. C,* 2014, **2**, 1730-1735.

[3] M. Jaymand, Polymer (Korea) 2010, **34**, 553-559.

[4] O. G. Reid, R. D. Pensack, Y. Song, G. D. Scholes and G. Rumbles, *Chem. Mater.,* 2014, **26**, 561-575.

[5] M. Khairy, *Synthetic. Met.,* 2014, **189**, 34-41.

[6] K. Abu-Rabeah, D. Atias, S. Herrmann, J. Frenkel, D. Tavor, S. Cosnier and R. S.Marks, *Langmuir,* 2009, **25**, 10384-10389.

[7] B. Guoa, L. Glavas and A. C. Albertsson, *Prog. Polym. Sci.,* 2013, **38**, 1263-1286.

[8] J. Leng, X. Lan, Y. Liu and S. Du, *Prog. Mater. Sci.,* 2011, **56**, 1077-1135.

[9] A. C. Carreon, W. L. Santos, J. B. Matson and R. C. So, *Polym. Chem.,* 2014, **5**, 314-317.

[10] K. Wang, H. Wu, Y. Meng and Z. Wei, *Small,* 2014, **10**, 14-31.

[11] M. Lanzi, L. Paganin and F. Errani, *Polymer,* 2012, **53**, 2134-2145.

[12] N. K. Guimard, N. Gomez and C. E. Schmidt, *Prog. Polym. Sci.,* 2007, **32**, 876-921.

[13] Y. Wang, H. D. Tran, L. Liao, X. Duan and R. B. Kaner, *J. Am. Chem. Soc.,* 2010, **132**, 10365-10373.

[14] M. Hatamzadeh, M. Jaymand and B. Massoumi, *Polym. Int.,* 2014, **63**, 402-412.

[15] M. Jaymand, *Design. Monomer. Polym.,* 2011, **14**, 433-444.

[16] M. Abbasian, M. Jaymand and S. E.Shoja-Bonab, *J. Appl. Polym. Sci.,* 2012, **125**, E131-E140.

[17] S. Ameen, M. Shaheer-Akhtar and M. Husain, *Sci. Adv. Mater.,* 2010, **2**, 441-462.

[18] Y. Chen, Y. Li, M. Yip and N. Tai, *Compos. Sci. Technol.,* 2013, **80**, 80-86.

[19] B. R. Kim, H. K. Lee, S. H. Park and H. K. Kim, *Thin. Solid. Film.,* 2011, **519**, 3492-3496.

[20] J. Azadmanjiri, P. Hojati-Talemi, G. P. Simon, K. Suzuki and C. Selomulya, *Polym. Eng. Sci.,* 2011, **51**, 247-253.

[21] B. R. Kim, H. K. Lee, E. Kim and S. H. Lee, *Synthetic. Met.,* 2010, **160**, 1838-1842.

[22] Y. S. Choi, Y. H. Yoo, J. G. Kim and S. H. Kim, *Surface. Coat. Technol.,* 2006, **201**, 3775-3782.

[23] Y. Zhao, S. Si and C. Liao, *J. Power. Sources.,* 2013, **241**, 449-453.

[24] I. Sultana, M. M. Rahman, S. Li, J. Wang, C. Wang, G. G. Wallace, H. K. Liu, *Electrochim. Acta.,* 2012, **60**, 201-205.

[25] G. Liu, S. Xun, N. Vukmirovic, X. Song, P. Olalde-Velasco, H. Zheng, V. S. Battaglia, L. Wang and W. Yang, *Adv. Mater.,* 2011, **23**, 4679-4683.

[26] K. C. Fang, C. P. Hsu, Y. W. Kang, J. Y. Fang, C. C. Huang, C. H. Hus, Y. F. Huang, C. C. Chen, S. S. Li, Y. J. Andrew, D. J. Yao and Y. L. Wang, *Biosensor. Bioelectronic.,* 2014, **55**, 294-300.

[27] H. C. Budnikov, G. A. Evtugyn and A. V. Porfireva, *Talanta,* 2012, **102**, 137-155.

[28] Z. Wang, C. Sun, G. Vegesna, H. Liu, Y. Liu, J. Li and X. Zeng, *Biosens. Bioelectron.,* 2013, **46**, 183-189.

[29] D. Bang, J. Lee, J. Park, J. Choi, Y. W. Chang, K. H. Yoo, Y. M. Huh and S. Haam, *J. Mater. Chem.,* 2012, **22**, 3215-3219.

[30] X. Li, Y. Wang, X. Yang, J. Chen, H. Fu, T. Cheng and Y. Wang, *Trend. Anal. Chem.,* 2012, **39**, 163-179.

[31] Q. Wu, M. Bhattacharya and S. E. Morgan, *ACS. Appl. Mater. Interfac.,* 2013, **5**, 6136-6146.

[32] O. Nahor, T. Segal-Peretz, L. Neeman, D. Oron and G. L. Frey, *J. Mater. Chem. C.,* 2014, **2**, 4167-4176.

[33] A. Iwan and A. Chuchmala, *Prog. Polym. Sci.,* 2012, **37**, 1805-1828.

[34] J. M. Spurgeon, M. G. Walter, J. Zhou, P. A. Kohl, N. S. Lewis, *Energ. Environ. Sci.,* 2011, **4**, 1772-1780.

[35] N. V. Blinova and F. Svec, *J. Membran. Sci.,* 2012, **423-424**, 514-521.

[36] P. D. Chapman, T. Oliveira, A. G. Livingston and K. Li, *J. Membran. Sci.,* 2008, **318**, 5-37.

[37] E. K. Chatzidaki, E. P. Favvas, S. K. Papageorgiou, N. K. Kanellopoulos and N. V. Theophilou, *Euro. Polym. J.,* 2007, **43**, 5010-5016.

[38] T. Ahuja, I. A. Mir, D. Kumar and Rajesh, *Biomaterials,* 2007, **28**, 791-805.

[39] A. D. Bendrea, G. Fabregat, J. Torras, S. Maione, L. Cianga, L. J. del Valle, I. Cianga and C. Aleman, *J. Mater. Chem B.,* 2013, **1**, 4135–4145.

[40] N. Kızılyar, N. Y. Ozden, L. Toppare and Y. Yagci, *Synthetic. Met.,* 1999, **104**, 45-50.

[41] H. Gomez, M. K. Ram, F. Alvi, E. Stefanakos and A. Kumar, *J. Phys. Chem., C,* 2010, **114**, 18797-18804.

[42] K. Qi, Y. Qiu, Z. Chen and X. Guo, *Corros. Sci.,* 2012, **60**, 50-58.

[43] R. S. Biscaro, M. C. Rezende and R. Faez, *Polym. Adv. Technol.,* 2009, **20**, 28-34.

[44] P. Saini, V. Choudhary, B. P. Singh, R. B. Mathur and S. K. Dhawan, *Mater. Chem. Phys.,* 2009, **113**, 919-926.

[45] A. Ohlan, K. Singh, A. Chandra and S. K. Dhawan, *Appl. Phys. Lett.,* 2008, **93**, 053114.

[46] T. Gurunathan, C. R. K. Rao, R. Narayan and K. V. S. N. Raju, *J. Mater. Sci.,* 2013, **48**, 67-80.

[47] R. S. Bobade, *J. Polym. Eng.,* 2011, **31**, 209-215.

[48] Z. Chen, R. Li and Q. Guo, *Appl. Mech. Mater.,* 2012, **217**, 1166-1169.

[49] J. Njuguna and K. Pielichowski, *J. Mater. Sci.,* 2004, **39**, 4081-4094.

[50] A. T. Ramaprasad, V. Rao and G. Sanjeev, *J. Appl. Polym. Sci.,* 2011, **121**, 623-633.

[51] D. A. Walker and C. D'Silva, *Electrochim. Acta.,* 2014, **116**, 175-182.

[52] T. Lindfors and R. M. Latonen, *Carbon,* 2014, **69**, 122-131.

[53] Y. Z. Long, M. M. Li, C. Gu, M. Wan, J. L. Duvail, Z. Liu and Z. Fan, *Prog. Polym. Sci.,* 2011, **36**, 1415-1442.

[54] L. A. P. Kane-Maguire and G. G. Wallace, *Chem. Soc. Rev.,* 2010, **39**, 2545-2576.

[55] M. I. Mangione, R. A. Spanevello, A. Rumbero, D. Heredia, G. Marzari, L. Fernandez, L. Otero and F. Fungo, *Macromolecules,* 2013, **46**, 4754-4763.

[56] B. Liang, Z. Qin, J. Zhao, Y. Zhang, Z. Zhou and Y. Lu, *J. Mater. Chem., A,* 2014, **2**, 2129-2135.

[57] S. M. Park and H. J. Lee, *Bull. Korean. Chem. Soc.,* 2005, **26**, 697-706.

[58] J. C. Vidal, E. Garcia-Ruiz and J. R. Castillo, *Microchim. Acta.,* 2003, **143**, 93-111.

[59] L. R. Nissen, N. W. Lepp and R. Edwards, *Chemosphere,* 2000, **41**, 265-269.

[60] S. Malamis and E. Katsou, *J. Hazard. Mater.,* 2013, **252-253**, 428-461.

[61] M. E. Davis, Chem. Mater., 2014, **26**, 239-245.

[62] N. Z. F. Mukhtar, S. Abdullah and M. M. Rusop, *Adv. Mater. Res.,* 2013, **667**, 53-57.

[63] A. Alberti, G. Cruciani, E. Galli, S. Merlino, R. Millini, S. Quartieri, G. Vezzalini and S. Zanardi, *J. Phys. Chem., B,* 2002, **106**, 10277-10284.

[64] G. T. Kokotailo, S. L. Lawton and D. H. Olson, *Nature,* 1978, **272**, 437-438.

[65] A. Alberti, G. Vezzalini, E. Galli and S. Quartieri, *Euro. J. Mineral.,* 1996, **8**, 69-75.

[66] K. Metropoulos, E. Maliou, M. Loizidou and N. Spyrellis, *J. Environ. Sci. Health., A,* 1993, **28**, 1507-1518.

[67] T. B. Reed and D. W. Breck, *J. Am. Chem. Soc.,* 1956, **78**, 5972-5977.

[68] G. Wu, H. Zhang, J. Zhou, A. Huang and Q. Wan, *J. Mater. Chem. C,* 2013, **1**, 5669-5674.

[69] P. Vanelderen, J. Vancauwenbergh, B. F. Sels and R. A. Schoonheydt, *Coordin. Chem. Rev.,* 2013, **257**, 483-494.

[70] L. Bonaccorsi, L. Calabrese and E. Proverbio, *Micropor. Mesopor. Mater.,* 2011, **144**, 40-45.

[71] T. Tago, H. Konno, Y. Nakasaka and T. Masuda, *Catal. Surv. Asia.,* 2012, **16**, 148-163.

[72] Z. Wang, J. Yu and R. Xu, *Chem. Soc. Rev.,* 2012, **41**, 1729-1741.

[73] A. Chojnacki, K. Chojnacka, J. Hoffmann and H. G. Orecki, *Miner. Eng.,* 2004, **17**, 933-937.

[74] G. F. Capra, M. G. Duras, S. Vacca, E. Grilli and A. Buondonno, *Micropor. Mesopor. Mater.,* 2013, **167**, 22-29.

[75] A. Nicula, D. Stamires and J. Turkevich, *J. Chem. Phys.,* 1965, **42**, 3684-3692.

[76] J. Cejka, H. van Bekkum, A. Corma and F. Schüth, Introduciton to zeolite science and practice, 3rd ed.; Elsevier: Amsterdam, 2007.

[77] S. Montalvo, L. Guerrero, R. Borja, E. Sánchez, Z. Milán, I. Cortés and M. A. Rubia, *Appl. Clay. Sci.,* 2012, **58**, 125-133.

[78] T. O. Drews and M. Tsapatsis, *Curr. Opin. Colloid. Interf. Sci.,* 2005, **10**, 233-238.

[79] S. Yao, Y. Zheng, S. Ng, L. Ding and H. Yang, *Appl. Catal., A,* 2012, **435-436**, 61-67.

[80] C. Jiang, L. Jia, Y. He, B. Zhang, G. Kirumba and J. Xie, *J. Colloid. Interf. Sci.,* 2013, **402**, 246-252.

[81] N. Ninan, S. Thomas and Y. Grohens, *Mater. Lett.,* 2014, **118**, 12-16.

[82] L. Yu, K. Dean and L. Li, *Prog. Polym. Sci.,* 2006, **31**, 576-602.

[83] M. Jaymand, *Polym. J.,* 2011, **43**, 186-193.

[84] M. Jaymand, *Polym. J.,* 2011, **43**, 901-908.

[85] M. Jaymand, *J. Polym. Res.,* 2011, **18**, 957-963.

[86] M. Jaymand, *J. Polym. Res.,* 2011, **18**, 1617-1624.

[87] R. Sengupta, M. Bhattacharya, S. Bandyopadhyay and A. K. Bhowmick, *Prog. Polym. Sci.,* 2011, **36**, 638-670.

[88] A. A. Azeez, K. Y. Rhee, S. J. Park and D. Hui, *Composites., B,* 2013, **45**, 308-320.

[89] P. Kiliaris and C. D. Papaspyrides. *Prog. Polym. Sci.,* 2010, **35**, 902-958.

[90] M. Jaymand, *Polymer,* 2011, **52**, 4760-4769.

[91] M. Jaymand, *Macromol. Res.,* 2011, **19**, 998-1005.

[92] N. Ballav and M. Biswas, *Mater. Sci. Eng., B,* 2006, **129**, 270-272.

[93] A. Rashidzadeh, A. Olad and S. Ahmadi, *Polym. Eng. Sci.,* 2013, **53**, 970-975.

[94] E. Flores-Loyola, R. Cruz-Silva, J. Romero-Garcıa, J. L. Angulo-Sanchez, F. F. Castillon and M. H.Farıas, *Mater. Chem. Phys.,* 2007, **105**, 136-141.

[95] G. M. Do-Nascimento and M. L. A. Temperini, *Euro. Polym. J.,* 2008, **44**, 3501-3511.

[96] G. J. Millar, G. F. Mc-Cann, C. M. Hobbis, G. A. Bowmaker and R. P. *Cooney. J. Chem. Soc., Faraday Transactions,* 1994, **90**, 2579-2584.

[97] P. Malkaj, E. Dalas, E. Vitoratos and S. Sakkopoulos, *J. Appl. Polym. Sci.,* 2006, **101**, 1853-1856.

[98] J. Kamonsawas, A. Sirivat, S. Niamlang, P. Hormnirun and W. Prissanaroon-Ouajai, *Sensors,* 2010, **10**, 5590-5603.

[99] K. Thuwachaowsoan, D. Chotpattananont, A. Sirivat, R. Rujiravanit and J. W. Schwank, *Mater. Sci. Eng., B,* 2007, **140**, 23-30.

[100] I. Sakellis, A. N. Papathanassiou and J. Grammatikakis, *J. Appl. Phys.,* 2009, **105**, 064109.

[101] E. Dalas, E. Vitoratos, S. Sakkopoulos and P. Malkaj, *J. Power. Sources.,* 2004, **128**, 319-325.

[102] A. Maity, N. Ballav and M. Biswas, *J. Appl. Polym. Sci.,* 2006, **101**, 913-921.

[103] E. Vitoratos, S. Sakkopoulos, E. Dalas, P. Malkaj and Ch. Anestis, *Curr. Appl. Phys.,* 2007, **7**, 578-581.

[104] S. Bocchini, A. Chiolerio, S. Porro, D. Accardo, N. Garino, K. Bejtka, D. Perrone and C. F. Pirri, *J. Mater. Chem. C,* 2013, **1**, 5101-5109.

[105] M. Jaymand, *Prog. Polym. Sci.,* 2013, **38**, 1287-1306.

[106] M. Hatamzadeh, A. Mahyar and M. Jaymand, *J. Braz. Chem. Soc.,* 2012, **23**, 1008-1017.

[107] G. Ciric-Marjanovic, V. Dondur, M. Milojevic, M. Mojovic, S. Mentus, A. Radulovic, Z. Vukovic and J. Stejskal, *Langmuir,* 2009, **25**, 3122-3131.

[108] H. L. Frisch, H. Song, J. Ma, M. Rafailovich, S. Zhu, N. L. Yang and X. Yan, *J. Phys. Chem., B,* 2001, **105**, 11901-11905.

[109] A. Olad and B. Naseri, *Prog. Org. Coat.,* 2010, **67**, 233-238.

[110] C. Chuapradit, L. Wannatong, D. Chotpattananont, P. Hiamtup, A. Sirivat and J. Schwank, *Polymer,* 2005, **46**, 947-953.

[111] N. Densakulprasert, L. Wannatong, D. Chotpattananont, P. Hiamtup, A. Sirivat and J. Schwank, *Mater. Sci. Eng., B,* 2005, **117**, 276-282.

[112] A. A. Shyaa, O. A. Hasan and A. M. Abbas, *J. Saudi. Chem. Soc.,* (Article in press; DOI:10.1016/j.jscs.2012.01.001).

[113] X. Ma, H. Xu, G. Li, M. Wang, H. Chen and S. Chen, *Macromol. Mater. Eng.,* 2006, **291**, 1539-1546.

[114] J. Jiang, Y. D. Liu, L. Shan, X. Zhang, Y. Meng, H. J. Choi and Y. Tian, *Smart. Mater. Struct.,* 2014, **23**, 015003.

[115] A. Ivan, S. K. Tanczos, O. Dorca, V. Danciulescu, S. Sava and G. Nechifor, *U.P.B. Sci. Bull., B,* 2013, **75,** 53-64.

[116] M. Milojevic-Rakic, A. Janosevic, J. Krstic, B. N. Vasiljevic, V. Dondur and G. Ciric-Marjanovic, *Micropor. Mesopor. Mater.,* 2013, **180**,141–155.

[117] Z. Safidine, Z. Ghebache and S. Lamouri, *Polym. J.,* 2013, **45**, 946–954.

[118] S. S. Shinde, G. S. Gund, V. S. Kumbhar, B. H. Patil and D. Lokhande, *Euro. Polym. J.,* 2013, **49**, 3734–3739.

[119] P. P. Jeeju, S. J. Varma, P. A. F. Xavier, A. M. Sajimol and S. Jayalekshmi, *Mater. Chem. Phys.,* 2013, **134**, 803-808.

[120] S. Chen and I. Zhitomirsky, *J. Power. Sources.,* 2013, **243**, 865-871.

[121] Y. Berdichevsky and Y. H. Lo, *Adv. Mater.,* 2006, **18**, 122-125.

[122] X. Du, X. Hao, Z. Wang, X. Ma, G. Guan, A. Abuliti, G. Ma and S. Liu, *Synthetic. Met.,* 2013, **175**, 138-145.

[123] R. Guo, G. Li, W. Zhang, G. Shen and D. Shen, *Chem. Phys. Phys. Chem.,* 2005, **6**, 2025-2028.

[124] L. Zuppiroli, F. Beuneu, J. Mory, P. Enzel and T. Bein, *Synthetic. Met.,* 1993, **57**, 5063-5068.

[125] B. Soontornworajit, L. Wannatong, P. Hiamtup, S. Niamlang, D. Chotpattananont, A. Sirivat and J. Schwank, *Mater. Sci. Eng., B,* 2007, **136**, 78-86.

[126] A. N. Papathanassiou, J. Grammatikakis, I. Sakellis, S. Sakkopoulos, E. Vitoratos and E. Dalas, *J. Appl. Phys.,* 2004, **96**, 3883.

[127] A. N. Papathanassiou, J. Grammatikakis, I. Sakellis, S. Sakkopoulos, E. Vitoratos and E. Dalas, *Synthetic. Met.,* 2005, **150**, 145-151.

[128] A. Matsumoto, T. Kitajima and K. Tsutsumi, *Langmuir,* 1999, **15**, 7626-7631.

[129] T. Bein and P. Enzel, *Angew. Chem. Int. Edit.,* 1989, **28**, 1692-1794.

[130] G. Cho, B. M. Fung, D. T. Glatzhofer, J. S. Lee and Y. G. Shul, *Langmuir,* 2001, **17**, 456-461.

[131] H. Uehara, M. Miyake, M. Matsuda and M. Sato, *J. Mater. Chem.,* 1998, **8**, 2133-2136.

[132] M. Trueba, A. L. Montero and J. Rieumont, *Electrochim. Acta.,* 2004, **49**, 4341-4349.

[133] M. Nakayama, J. Yano, K. Nakaoka and K. Ogura, *Synthetic. Met.,* 2003, **138**, 419-422.

[134] L. Wannatong and A. Sirivat, *Reac. Funct. Polym.,* 2008, **68**, 1646-1651.

[135] R. Wang, T. Zhang, Y. He, X. Li, W. Geng, J. Tu and Q. Yuan, *J. Appl. Polym. Sci.,* 2010, **115**, 3474-3480.

[136] A. Olad, Sh. Ahmadi and A. Rashidzadeh, *Desalin. Water. Treat.,* 2013, **51**, 7172-7180.

[137] H. Javadian and M. Taghavi, *Appl. Surface. Sci.,* 2014, **289**, 487-494.

[138] D. Aradilla, F. Estrany, F. Casellas, J. I. Iribarren and C. Alemán. *Org. Electron.,* 2014, **15**, 40–46.

[139] T. Higashihara and M. Ueda, *Macromol. Res.,* 2013, **21**, 257-271.

[140] K. Kawabata, M. Takeguchi and H. Goto, *Macromolecules,* 2013, **46**, 2078–2091.

[141] L. Cardenas, R. Gutzler, J. Lipton-Duffin, C. Fu, J. L. Brusso, L. E. Dinca, M. Vondráček, Y. Fagot-Revurat, D. Malterre, F. Rosei and D. F. Perepichka, *Chem. Sci.,* 2013, **4**, 3263-3268.

[142] C. Li and G. Shi, *ACS. Appl. Mater. Interfaces.,* 2013, **5**, 4503-4510.

[143] M. Shao, Y. He, K. Hong, C. M. Rouleau, D. B. Geohegan and K. Xiao, *Polym. Chem.,* 2013, **4**, 5270-5274.

[144] M. Hatamzadeh and M. Jaymand, *RSC Adv.,* 2014, **4**, 16792–16802.

[145] B. Massoumi, M. Jaymand, R. Samadi and A. A. Entezami, *J. Polym. Res.,* 2014, **21**, 442.

[146] T. Nishinaga and K. Komatsu, *Org. Biomolecul. Chem.,* 2005, **3**, 561-569.

[147] A. Malinauskas, *Polymer,* 2001, **42**, 3957-3972.

[148] C. Eylem and J. A. Hriljac, *Chem. Mater.,* 1996, **8**, 844-849.

[149] P. Enzel and T. Bein, *Synthetic. Met.,* 1993, **55**, 1238-1245.

[150] G. Cıka, F. Sersenb and A. Bumbalovac, *Micropor. Mesopor. Mater.,* 2001, **46**, 81-86.

[151] G. Cıka, S. Priesolova, H. Bujdakova, F. Sersen, T. Potheoova and J. Kristın, *Chemosphere,* 2006, **63**, 1419-1426.

[152] M. Arvand, R. Ansari and L. Heydari, *Mater. Sci. Eng., C,* 2011, **31**, 1398-1404.

[153] N. Ballav and M. Biswas. *Mater. Sci. Eng., B,* 2006, **129**, 270-272.

[154] G. F. Mc-Cann, G. J. Millar, G. A. Bowmaker and R. P. Cooney, *J. Chem. Soc., Faraday Transactions,* 1995, **91**, 4321-4328.

[155] J. Kamonsawas, A. Sirivat and P. Hormnirun, *Int. J. Polym. Mater. Polym. Biomater.,* 2013, **62**, 583-589.

[156] N. F. Atta, M. F. El-Kady and A. Galal, *Sensors. Actuator., B,* 2009, **141**, 566-574.

[157] V. Hernandez, F. J. Ramirez, G. Zotti and J. T. Lopez, *Chem. Phys. Lett.,* 1992, **191**, 419-422.

[158] N. Ballav and M. Biswas, *Polym. Int.,* 2005, **54**, 725-729.

[159] E. Nazarzadeh-Zare, M. Mansour-Lakouraj, P. Najafi-Moghadam and R. Azimi, *Polym. Compos.,* 2013, **34**, 732-739.

[160] T. Ohsawa, K. Kaneto and K. Yoshino, *Japan. J. Appl. Phys.,* 1984, **23**, L663-665.

[161] M. J. Gonzalez-Tejera, E. Sanchez de la Blanca and I. Carrillo, *Synthetic. Met.,* 2008, **158**, 165-189.

[162] S. Sena, B. Bardakcıb, A. G. Yavuzc and A. U. Gokc, *Euro. Polym. J.,* 2008, **44**, 2708-2717.

[163] P. S. Sardar, S. Ghosh, M. Biswas, N. Ballav, *Polym. J.,* 2008, **40**, 1199-1203.

[164] P. Phumman, S. Niamlang and A. Sirivat, *Sensors,* 2009, **9**, 8031-8046.

Abbreviations

ICP, intrinsically conductive polymer; CPs, conducting polymers; PTh, polythiophene; PPy, polypyrrole; PANI, polyaniline; EMI, electromagnetic interference; AS, FTIR, aluminosilicates; Fourier transform infrared spectroscopic; XRD, X-ray diffraction; SEM, scanning electron microscopy; N *K* XANES, X-ray absorption near edge spectroscopy at the nitrogen K edge; CO, carbonmonoxide; MA, maleic acid; ^{1}H NMR, proton nuclear magnetic resonance spectroscopy; TGA, thermogravimetric analysis; CPC, cetylpyridinium chloride; TEM, transmission electron microscopy; SAAs, self-assembled arrays; EPR, electron paramagnetic resonance; DTA, differential thermal analysis; ESR, electron spin resonance; dc, direct-current; ac, alternating-current; ROS, reactive oxygen species; ISE, ion-selective electrode; dPPV, doped poly(*para*-phenylene vinylene); MEK, methyl ethyl ketone; MIBK, 4-methylpentan-2-one; APS, ammonium peroxydisulfate; PPP, poly(*p*-phenylene).

Schemes and Figures Captions:

Scheme 1. Three different types of basic polyaniline.

Scheme 2. Proposed mechanism by Densakulprasert et al. for the CO-PANI interaction [111].

Figure 1. SEM images of (A) pure PANI and (B) PANI/zeolite nanocomposite [112].

Figure 2. The effect of pH on the removal efficiency of Cr(VI) (the initial concentration, volume of solution and the amount of adsorbent were 50 ppm, 50 mL and 0.2 g, respectively) [112].

Figure 3. pH response of the PPy/zeolite–Pt electrode and PA/zeolite–Pt electrode [97].

Figure 4. The SEM images of zeolite 5A (a, b), and polyaniline/zeolite 5A composite (c, d) at different magnifications [115].

Scheme 3. Synthesis of PPy via chemical oxidation polymerization using $CuCl_2$ as an oxidant and description of redox reaction of PPy.

Figure 5. Descriptive illustration for preparation of core-shell polypyrrole/TS-1 zeolite nanocomposites by Cho et al. [130].

Figure 6. SEM micrographs of the pure PPy (a), pristine clinoptilolite (b), and PPy/Clino nanocomposite [93].

Figure 7. Cyclic voltammograms of PPy/clino nanocomposite in HCl electrolyte (1M) at the potential scan rates of 25, 50, and 100 mV s^{-1} [93].

Figure 8. Frequency dependences of electrical conductivities of pyrrole/1.0Cu-NaY (■), NaY (□), pyrrole/1.0Cu-USY(●), and USY (○) [131].

Figure 9. Electron spin resonance (ESR) spectra of PPy/Y-zeolite composite (a) and pure PPy (b) films. Both films were prepared by applying an electrical charge of 49 mC cm^{-2} [133].

Figure 10. Sensitivity of four sensing materials toward vapor of acetone, MEK, methanol, and toluene, at 3 vol% in N_2 [134].

Figure 11. Scanning electron microscopy images of SBA-15 (a) and NiO–PPy/SBA-15 (b) [135].

Figure 12. Results of the dc circuit test: (a) low-humidity conditions and (b) high-humidity conditions I, direct current [135].

Figure 13. The effects of contact time on the removal efficiency of Ni(II) [136].

Figure 14. The effects of pH on the removal efficiency of Ni(II) [136].

Figure 15. The effect of temperature on removal efficiency of mercury ions [137].

Figure 16. The results obtained for reusing the PPy/SH-Beta/MCM-41 after desorption [137].

Scheme 4. Probable mechanism for oxidative polymerization of thiophene.

Figure 17. Dependency of the number of live cells of bacterium S. *aureus* on the weight of the photocatalyst (texp = 16 hours) [151].

Figure 18. Dependency of the number of live cells of bacterium E. *coli* on the weight of the photocatalyst (texp = 16 hours) [151].

Figure 19. Scanning electron micrographs of Y-zeolite (a) and PTh/Y-zeolite composite (b) and transmission electron micrograph of PTh/Y-zeolite composite (c) [152].

Figure 20. Potential responses of various ISEs based on PTh/Y-zeolite composite for each anion separately [152].

Scheme 5. Response mechanism of the sulfide ion-selective electrode based on PTh/Y-zeolite composite. Ⓩ represents Y-zeolite [152].

Figure 21. SEM images of 13X-zeolite (a) and PTh/13X-zeolite composite (b) [153].

Scheme 6. Proposed mechanism by Thuwachaowsoan et al. for the H_2-P3TAA interaction [99].

Figure 22. The morphology of dPPV, NH_4^+ Y powders, and dPPV_[90] NH_4^+ Y composites at 10% v/v of dPPV: (a) dPPV at magnification of 1000×; (b) Zeolite Y at magnification 5000×; (c) dPPV_[90] NH_4^+ Y at magnification of 2000×; and (d) dPPV_[90] NH_4^+ Y at magnification of 5000× [155].

Figure 23. The sensitivity values of dPPV, dPPV_[90]HY, dPPV_[90]NaY, and dPPV_[90] NH_4^+ Y, when exposed to acetone, methyl ethyl ketone (MEK) and 4-methylpentan-2-one (MIBK) at 25 °C, 1 atm, and at the solvent concentration of 30000 ppm in N_2 [155].

Scheme 7. Suggested chemical structure of linear polyfuran.

Figure 24. TGA scans for 13X(■), PFu/13X(●) (loading of PFu is 80%), PANI-PFu/13X(▲) (loading of PFu is 80% and PANI is 65%) and PFu(▼) [163].

Schemes and Figures:

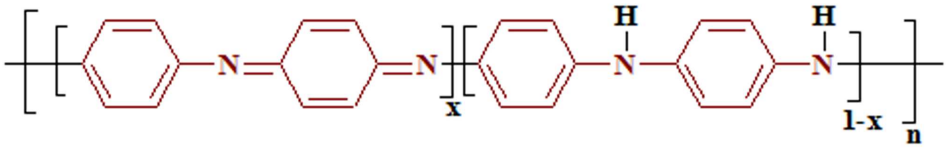

LEB : X = 0 ; EB : X = 0.5 ; PAB : X = 1

Scheme 1. Three different types of basic polyaniline.

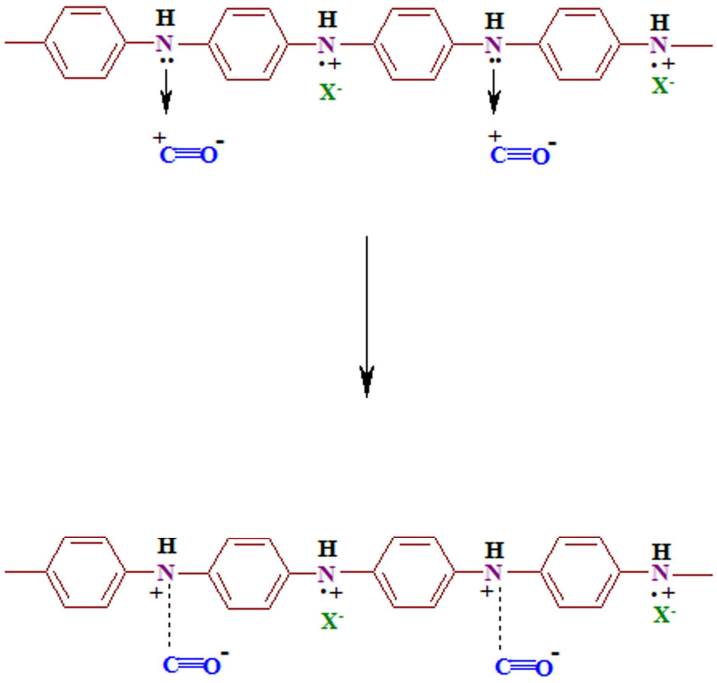

Scheme 2. Proposed mechanism by Densakulprasert et al. for the CO-PANI interaction [111].

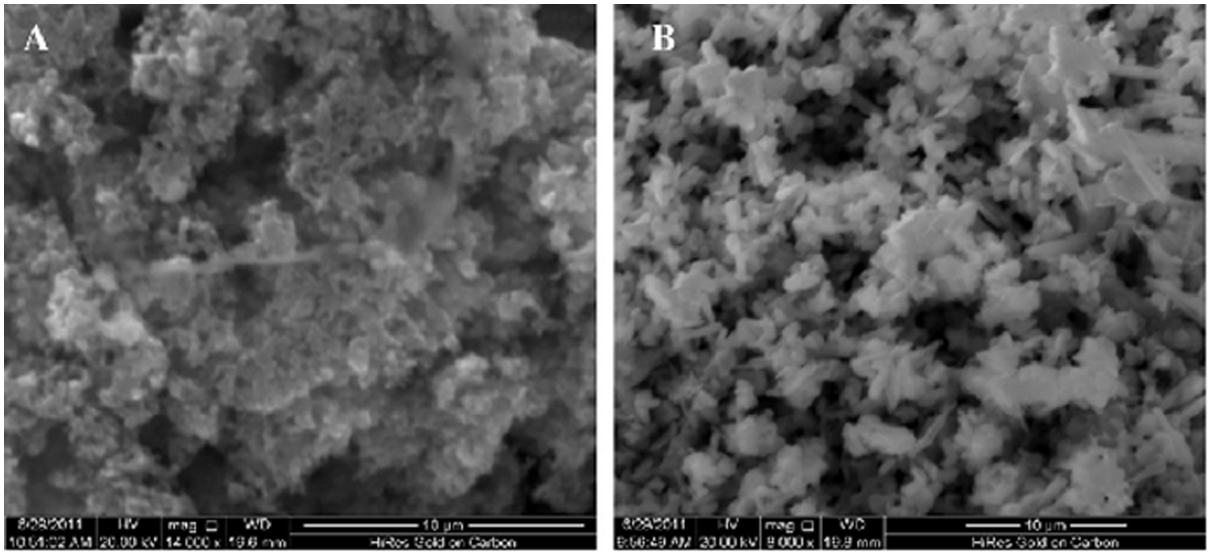

Figure 1. SEM images of (A) pure PANI and (B) PANI/zeolite nanocomposite [112].

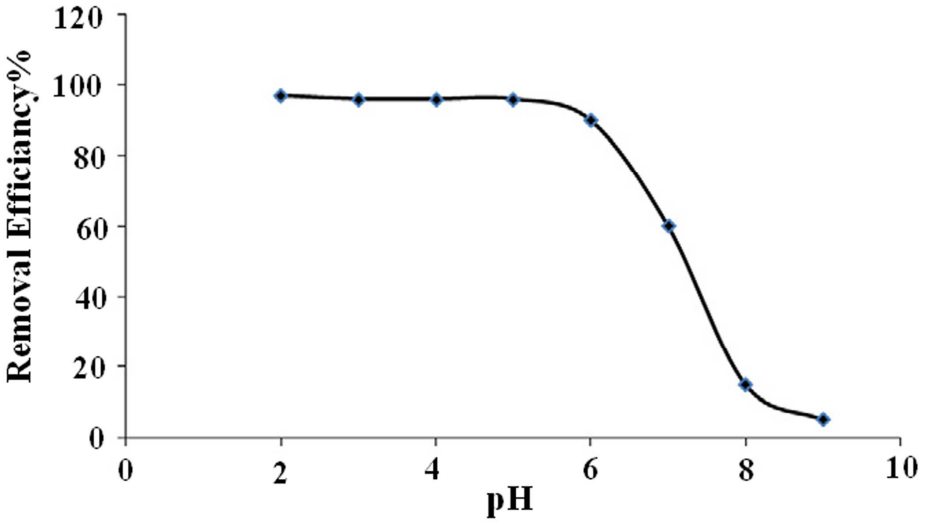

Figure 2. The effect of pH on the removal efficiency of Cr(VI) (the initial concentration, volume of solution and the amount of adsorbent were 50 ppm, 50 mL and 0.2 g, respectively) [112].

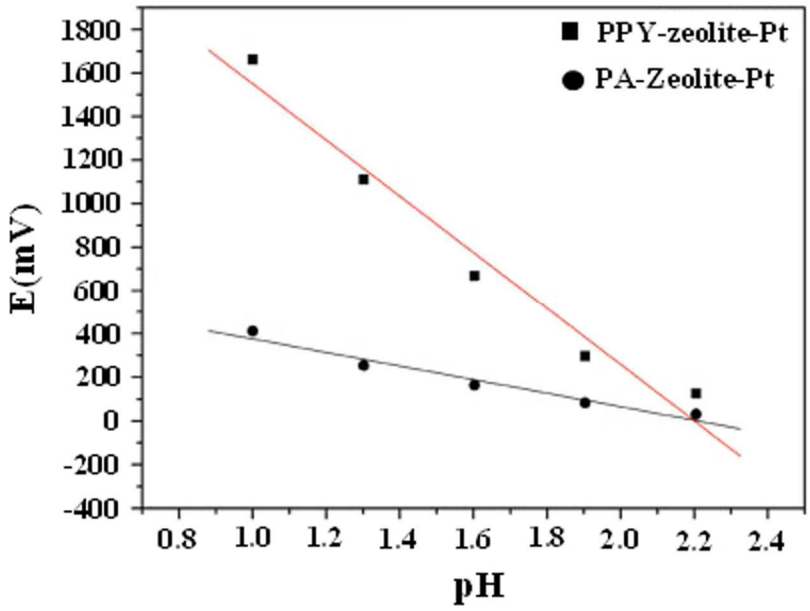

Figure 3. pH response of the PPy/zeolite–Pt electrode and PA/zeolite–Pt electrode [97].

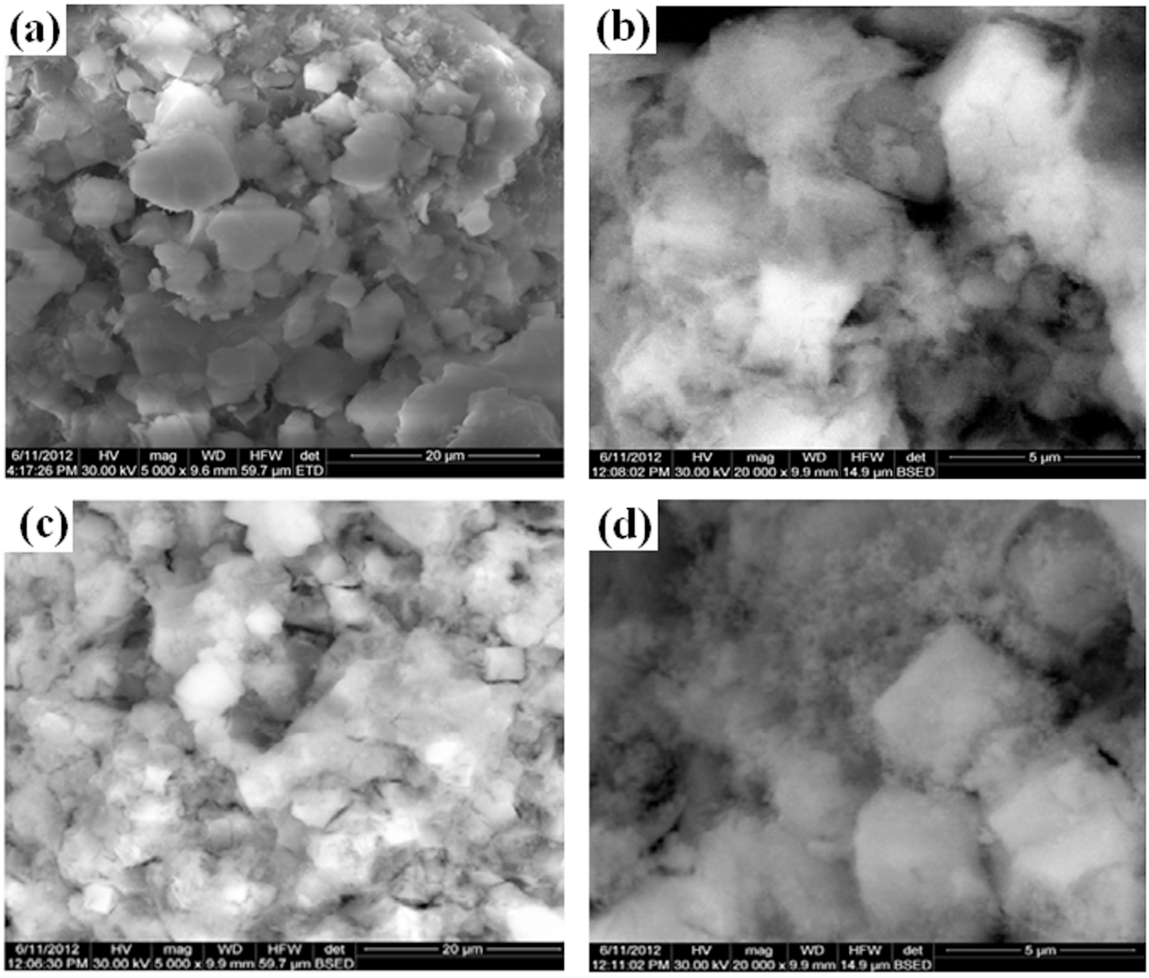

Figure 4. The SEM images of zeolite 5A (a, b), and polyaniline/zeolite 5A composite (c, d) at different magnifications [115].

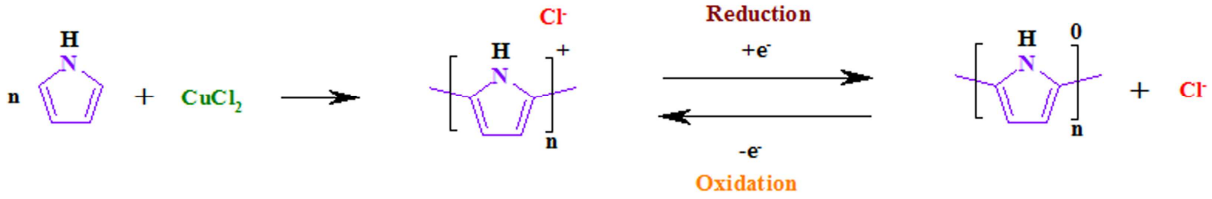

Scheme 3. Synthesis of PPy via chemical oxidation polymerization using $CuCl_2$ as an oxidant and description of redox reaction of PPy.

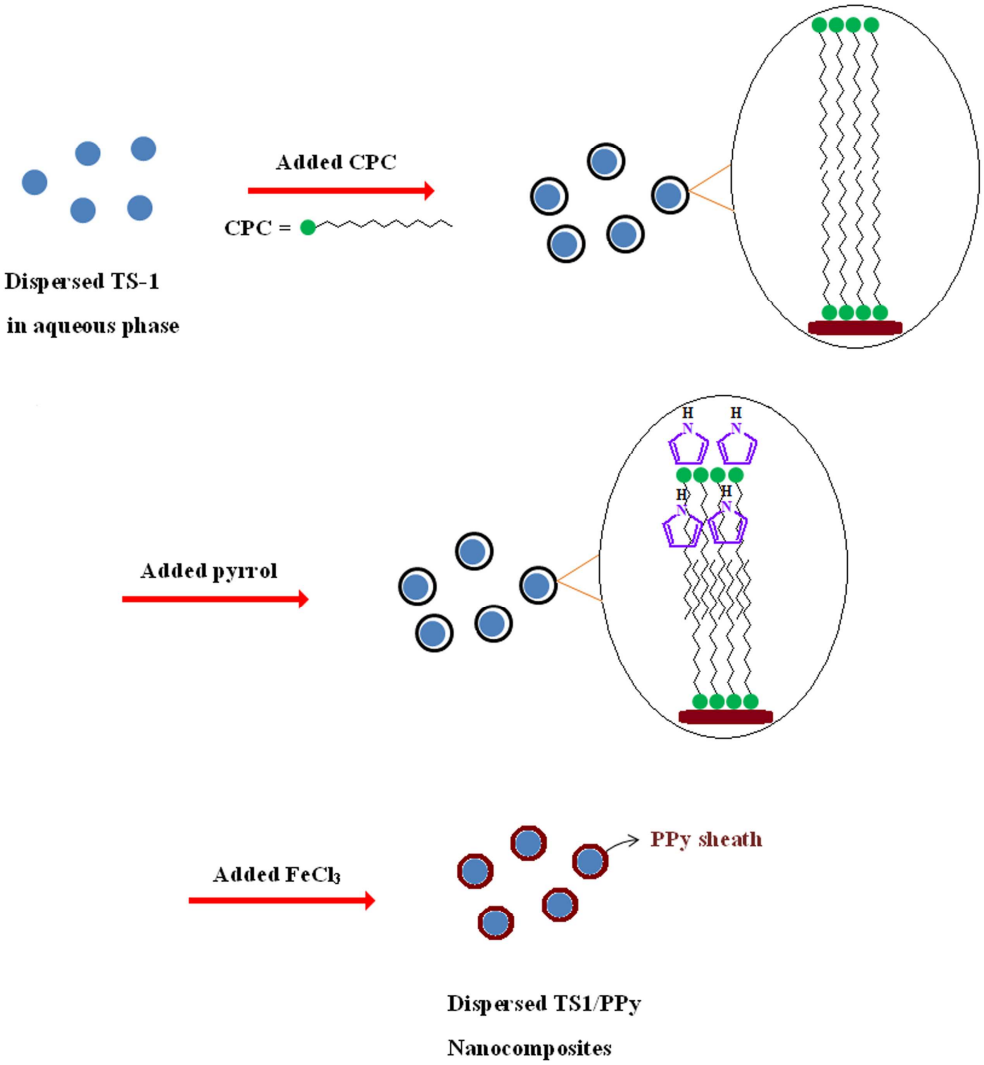

Figure 5. Descriptive illustration for preparation of core-shell polypyrrole/TS-1 zeolite nanocomposites by Cho et al. [130].

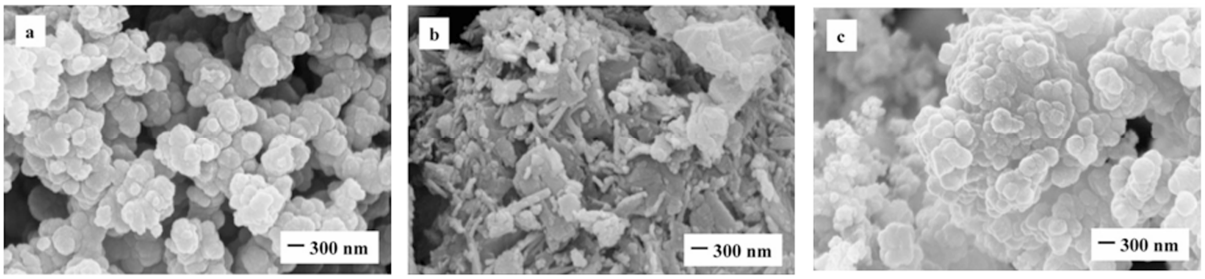

Figure 6. SEM micrographs of the pure PPy (a), pristine clinoptilolite (b), and PPy/Clino nanocomposite [93].

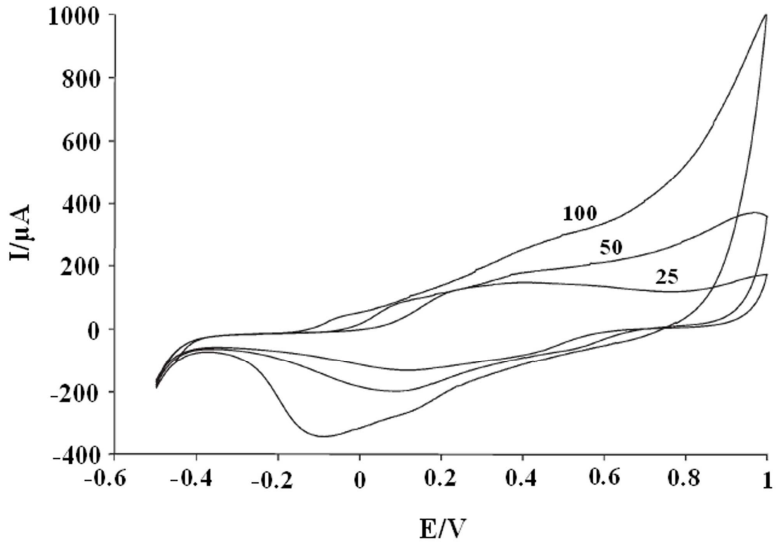

Figure 7. Cyclic voltammograms of PPy/clino nanocomposite in HCl electrolyte (1M) at the potential scan rates of 25, 50, and 100 mV s^{-1} [93].

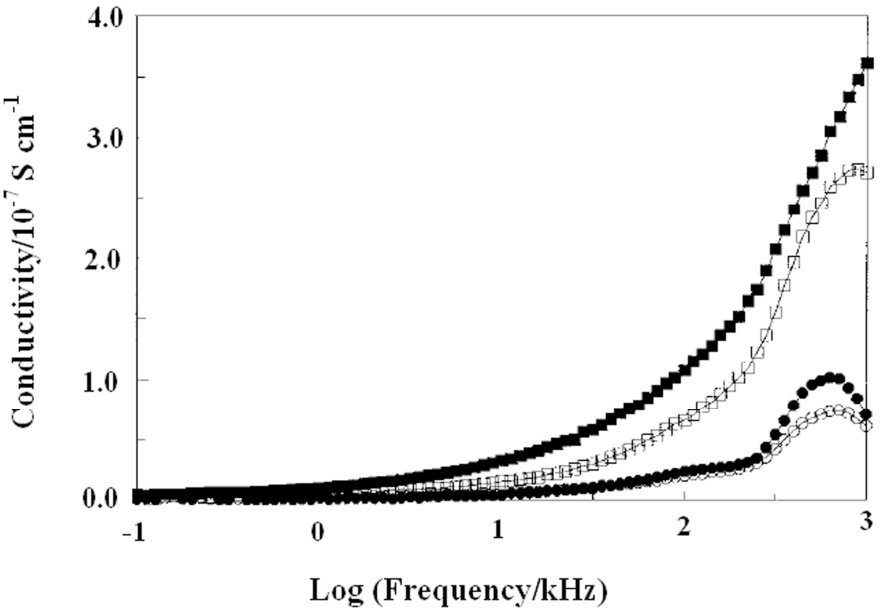

Figure 8. Frequency dependences of electrical conductivities of pyrrole/1.0Cu-NaY (■), NaY (□), pyrrole/1.0Cu-USY(●), and USY (○) [131].

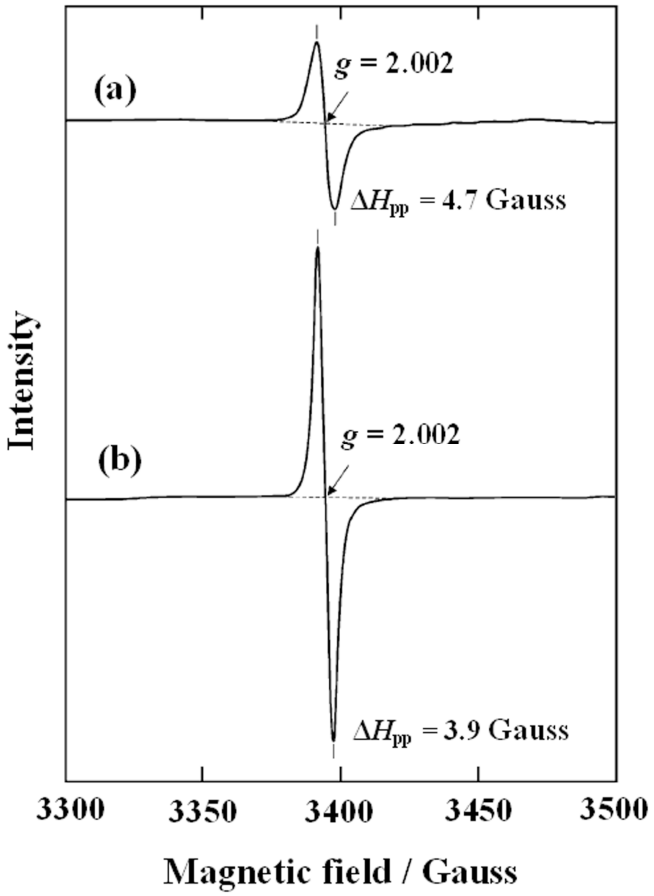

Figure 9. Electron spin resonance (ESR) spectra of PPy/Y-zeolite composite (a) and pure PPy (b) films. Both films were prepared by applying an electrical charge of 49 mC cm^{-2} [133].

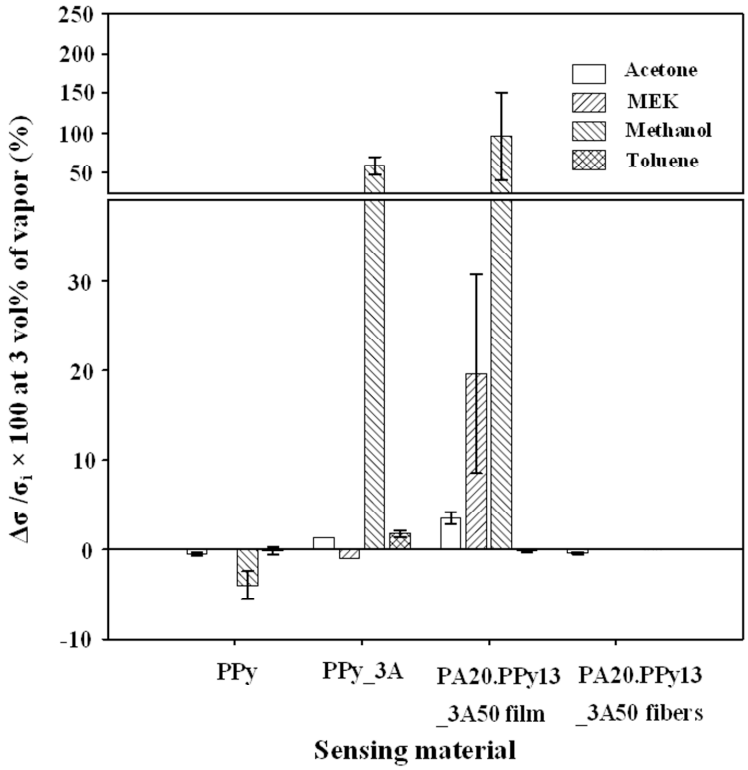

Figure 10. Sensitivity of four sensing materials toward vapor of acetone, MEK, methanol, and toluene, at 3 vol% in N_2 [134].

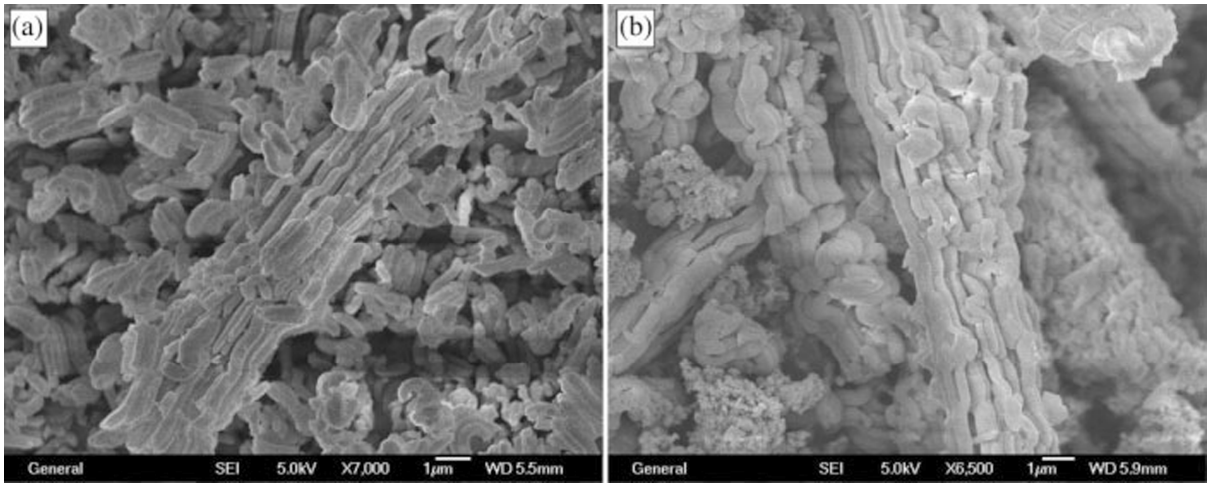

Figure 11. Scanning electron microscopy images of SBA-15 (a) and NiO–PPy/SBA-15 (b) [135].

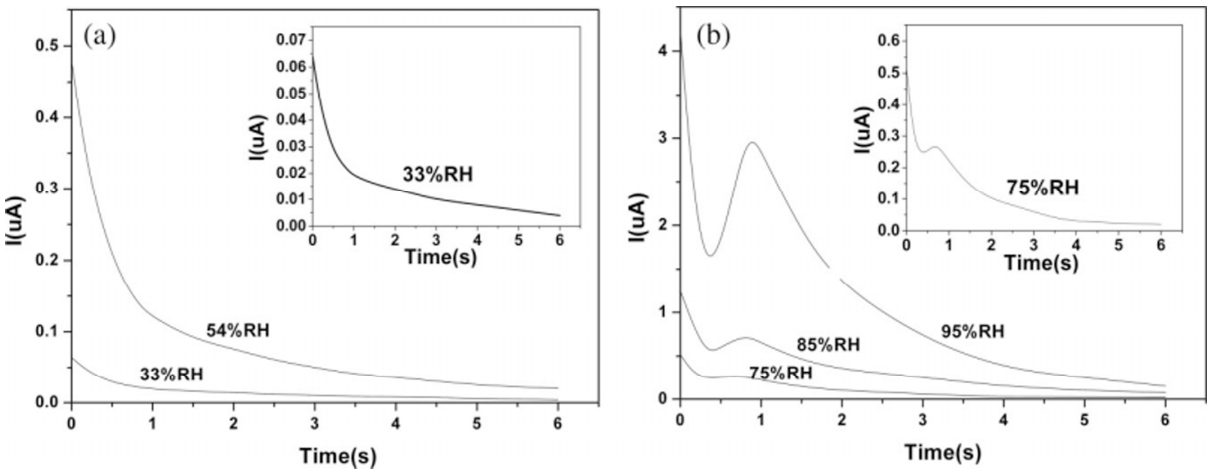

Figure 12. Results of the dc circuit test: (a) low-humidity conditions and (b) high-humidity conditions I, direct current [135].

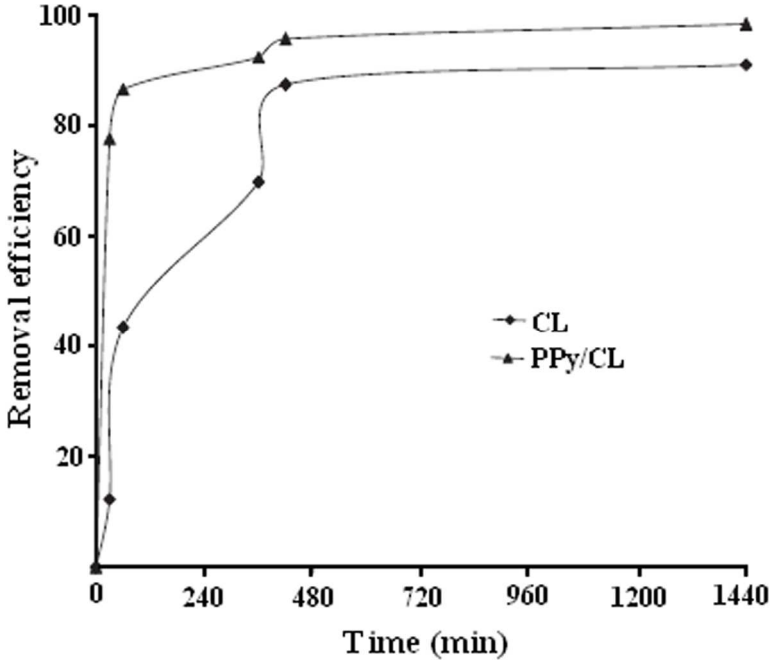

Figure 13. The effects of contact time on the removal efficiency of Ni(II) [136].

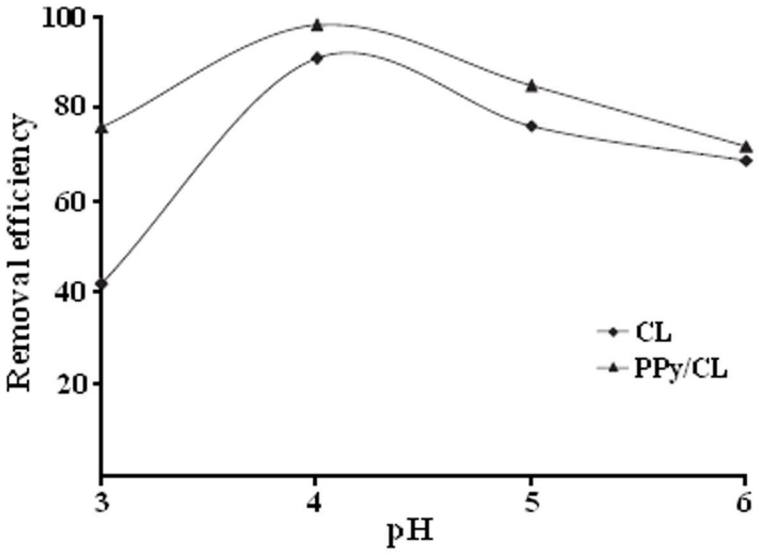

Figure 14. The effects of pH on the removal efficiency of Ni(II) [136].

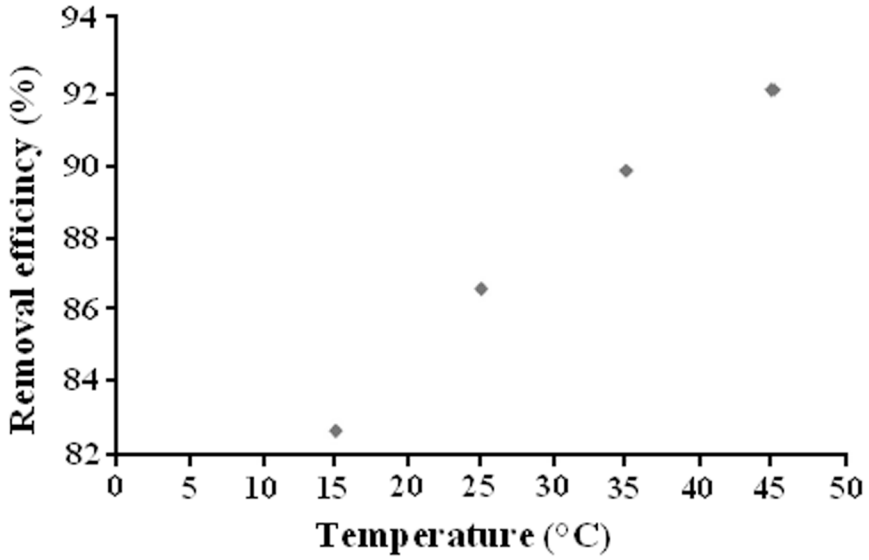

Figure 15. The effect of temperature on removal efficiency of mercury ions [137].

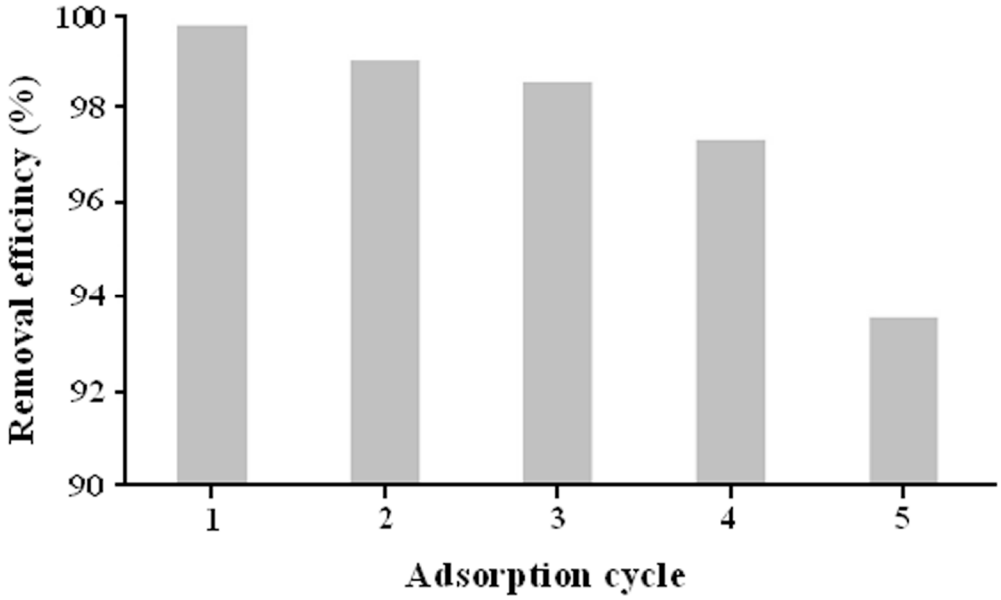

Figure 16. The results obtained for reusing the PPy/SH-Beta/MCM-41 after desorption [137].

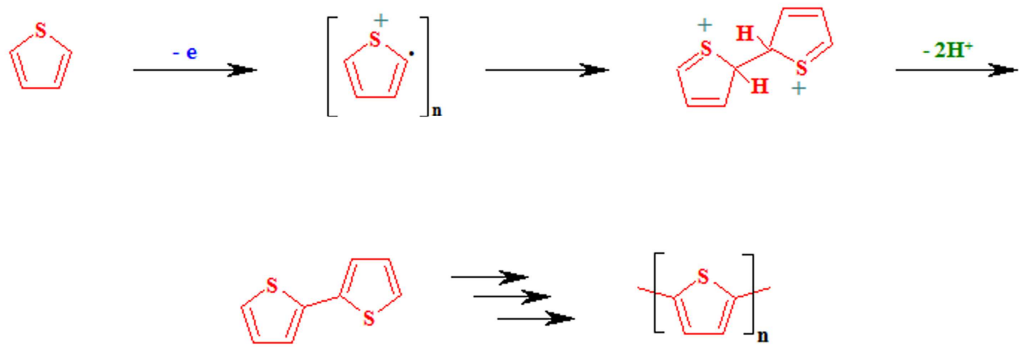

Scheme 4. Probable mechanism for oxidative polymerization of thiophene.

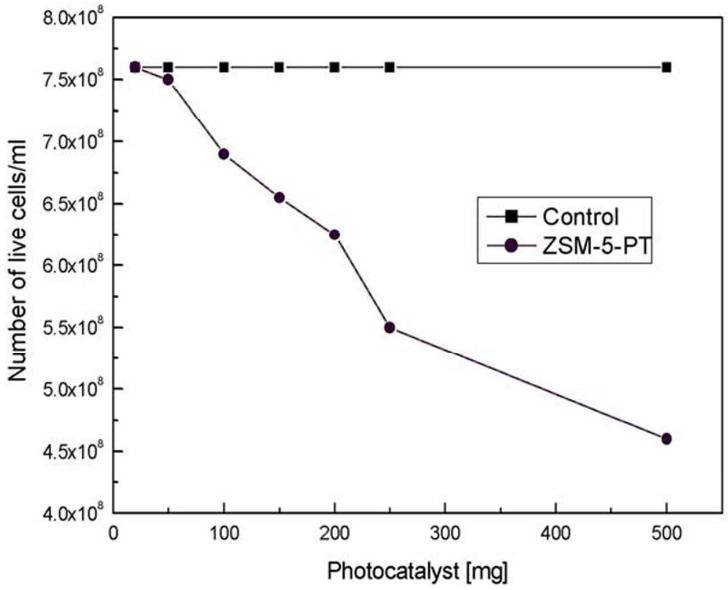

Figure 17. Dependency of the number of live cells of bacterium S. *aureus* on the weight of the photocatalyst (texp = 16 hours) [151].

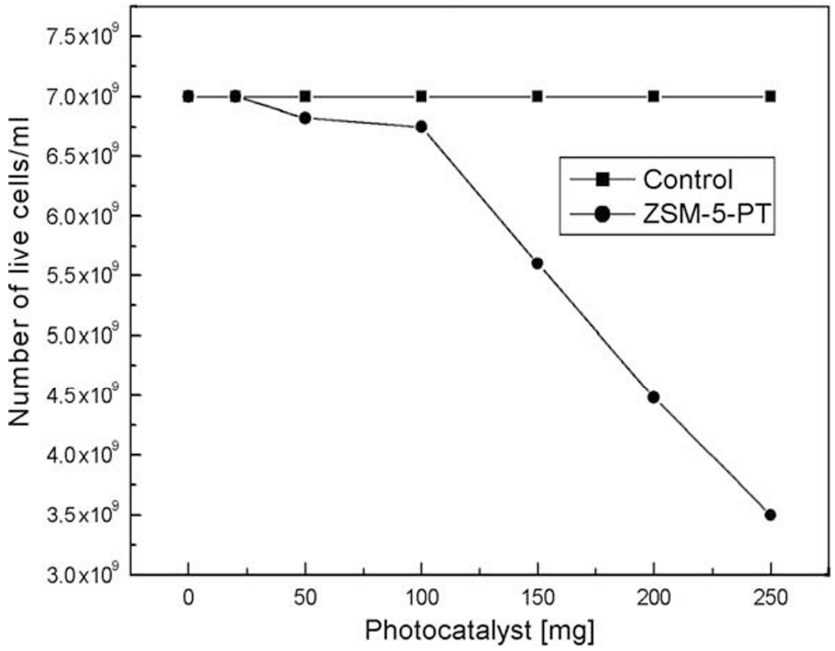

Figure 18. Dependency of the number of live cells of bacterium E. *coli* on the weight of the photocatalyst (texp = 16 hours) [151].

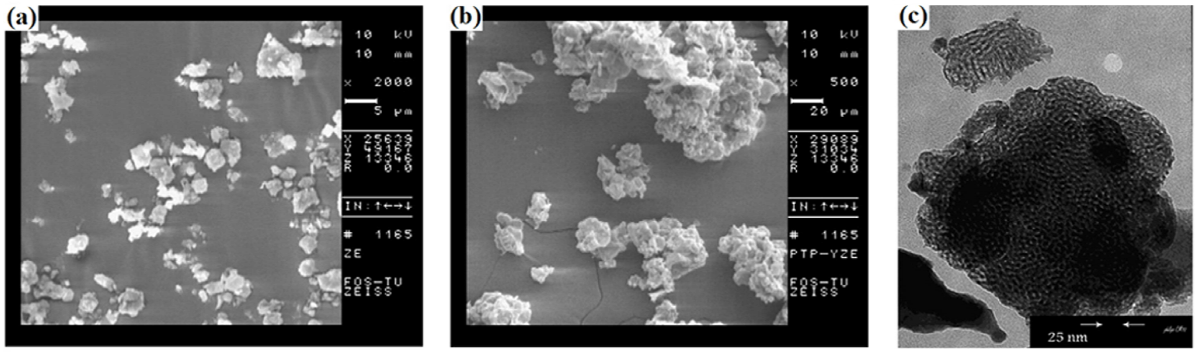

Figure 19. Scanning electron micrographs of Y-zeolite (a) and PTh/Y-zeolite composite (b) and transmission electron micrograph of PTh/Y-zeolite composite (c) [152].

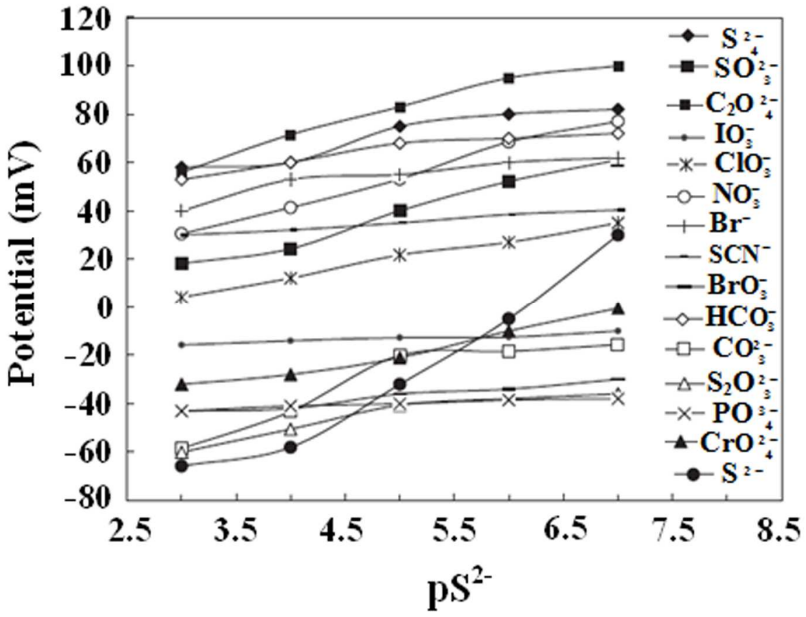

Figure 20. Potential responses of various ISEs based on PTh/Y-zeolite composite for each anion separately [152].

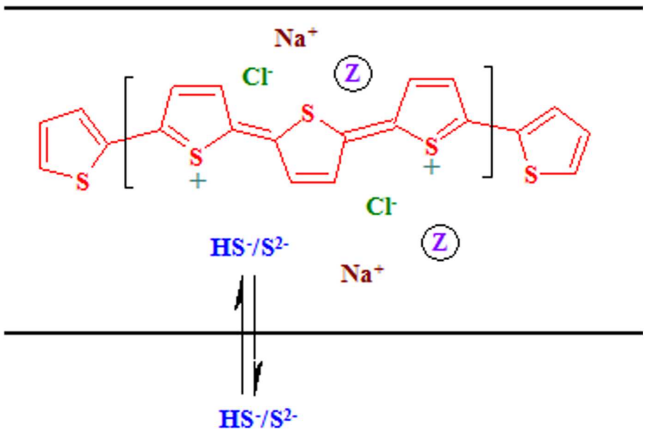

Scheme 5. Response mechanism of the sulfide ion-selective electrode based on PTh/Y-zeolite composite. ⓩ represents Y-zeolite [152].

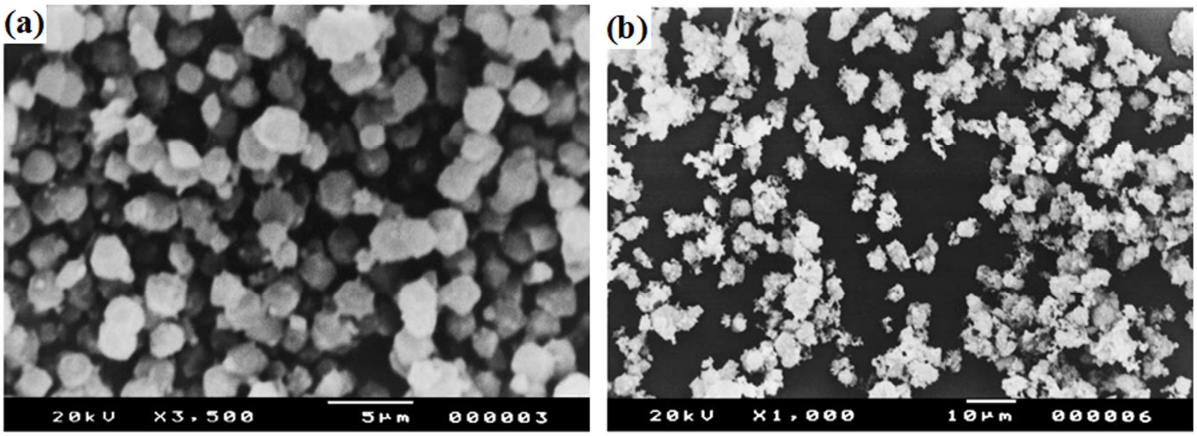

Figure 21. SEM images of 13X-zeolite (a) and PTh/13X-zeolite composite (b) [153].

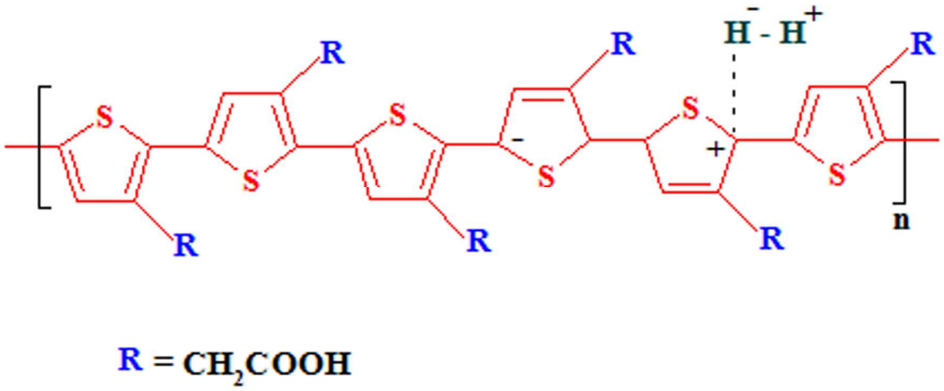

Scheme 6. Proposed mechanism by Thuwachaowsoan et al. for the H_2-P3TAA interaction [99].

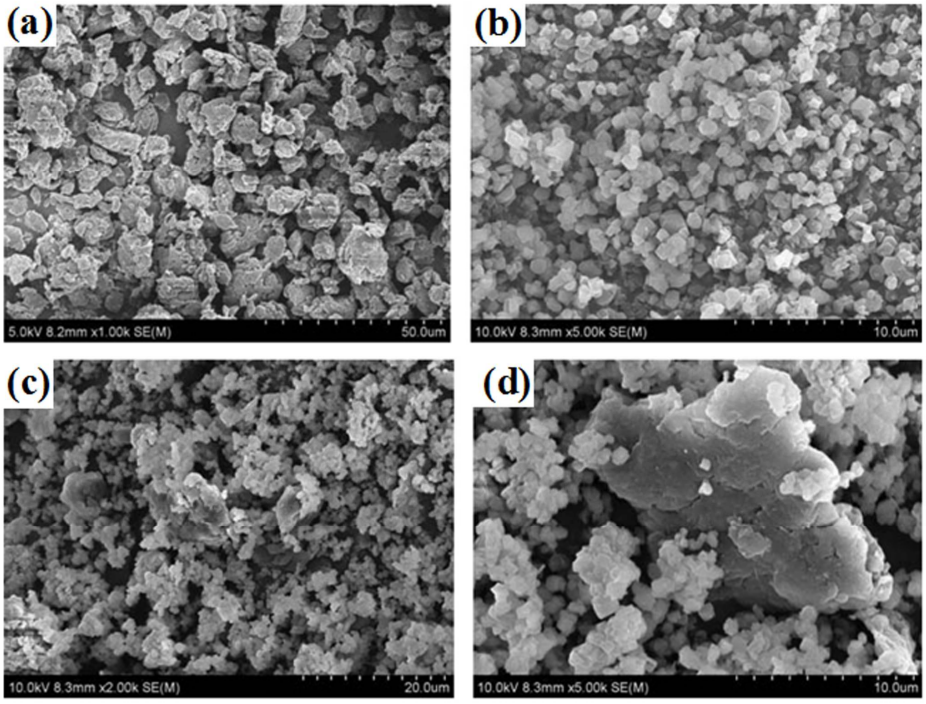

Figure 22. The morphology of dPPV, NH_4^+ Y powders, and dPPV_[90] NH_4^+ Y composites at 10% v/v of dPPV: (a) dPPV at magnification of 1000×; (b) Zeolite Y at magnification 5000×; (c) dPPV_[90] NH_4^+ Y at magnification of 2000×; and (d) dPPV_[90] NH_4^+ Y at magnification of 5000× [155].

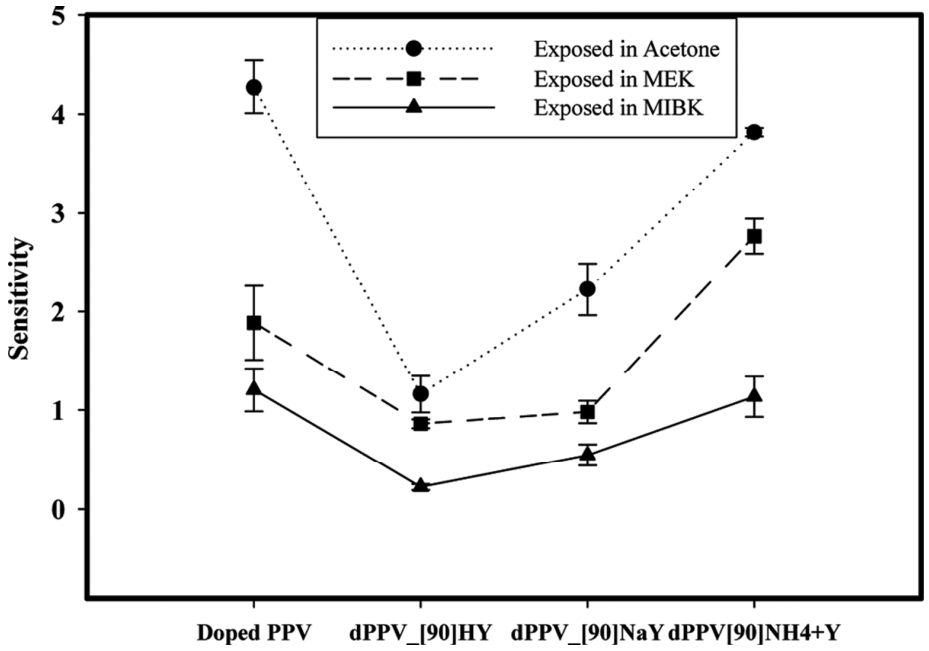

Figure 23. The sensitivity values of dPPV, dPPV_[90]HY, dPPV_[90]NaY, and dPPV_[90] NH_4^+ Y, when exposed to acetone, methyl ethyl ketone (MEK) and 4-methylpentan-2-one (MIBK) at 25 °C, 1 atm, and at the solvent concentration of 30000 ppm in N_2 [155].

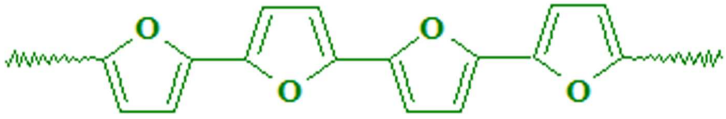

Scheme 7. Suggested chemical structure of linear polyfuran.

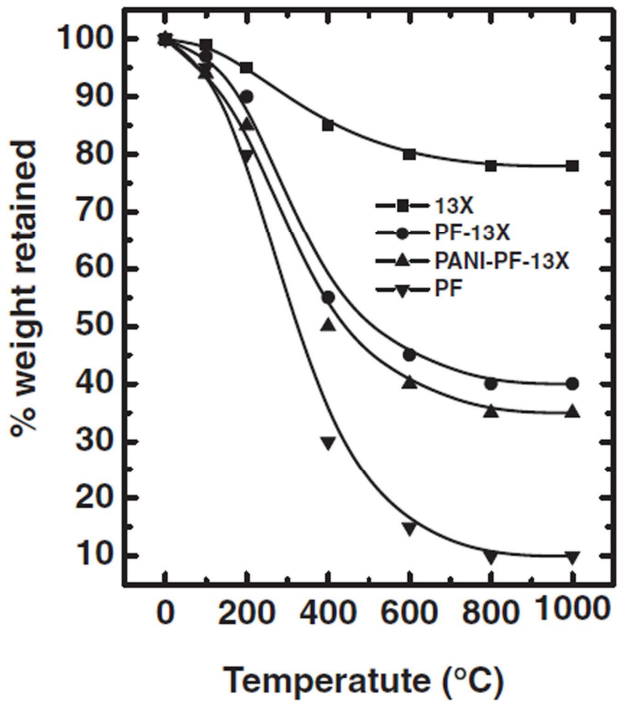

Figure 24. TGA scans for 13X(■), PFu/13X(●) (loading of PFu is 80%), PANI-PFu/13X(▲) (loading of PFu is 80% and PANI is 65%) and PFu(▼) [163].

Tables Captions:

Table 1. Conductivity values of MOR-Cu(II) and ZY-Cu(II) before and after the exposition to aniline and HCl vapors [95].

Table 2. The medium flux and retention of the dynamic membranes for cobalt ions [115].

Table 3. Peak widths of the organic radical EPR signal observed after reaction of thiophene and pyrrole in HM, L, M and H [154][a].

Table 4. Some typical data on the polymerization of furan in the presence of 13X zeolite [163].

Table 5. Some typical data on the formation PANI-PF/13X composite [163].

Tables:

Table 1. Conductivity values of MOR-Cu(II) and ZY-Cu(II) before and after the exposition to aniline and HCl vapors [95].

Inorganic porous hosts	Conductivity (S cm^{-1})	Conductivity ($S.cm^{-1}$): after exposition of aniline and HCl vapors	Variation Δp
MOR-Cu(II)	1.8×10^{-9}	2.8×10^{-9}	1.5
ZY-Cu(II)	2.9×10^{-8}	4.5×10^{-3}	1.5×10^{5}

Table 2. The medium flux and retention of the dynamic membranes for cobalt ions [115].

Membranes	Flux (L/m^2 h)	Retention (%)
Zeolite	151.42	67.58
PANI	126.36	77.43
PANI/Zeolite	118.87	98.20

Table 3. Peak widths of the organic radical EPR signal observed after reaction of thiophene and pyrrole in HM, L, M and H [154][a].

	peak width/G	
sample	thiophene	pyrrole
H	12.6 (2 h)	10 (7 h)
M	13.8 and 9.6	16.3 and 11.3
L	11	11.3
HM	21.3 and 26	18.2 and 15.7

[a] The three samples are referred to as low, medium and high copper mordenite (L, M, H). Calcined, outgassed H^+-mordenite (CBV 20A) was also studied as a substrate and is referred to as HM.

Table 4. Some typical data on the polymerization of furan in the presence of 13X zeolite [163].

Entry.No.	Reactants (g)			Products	
	Furan	$FeCl_3$	13X	Composite (g)	Loading of PFu (%)
1	1.0	1.0	1.0	1.40	70.3
2	2.0	2.0	2.0	2.75	68.7
3	1.0	1.0	1.0	1.60	80.0

Table 5. Some typical data on the formation PANI-PF/13X composite [163].

Entry.No.	Reactants (g)			Products	
	ANI	APS	PFu/13X[a]	Composite (g)	Loading of PANI (%)
1	0.25	-	0.50	0.53	12.0
2	0.50	-	0.50	0.96	47.9
3	0.75	-	0.50	1.43	65.1

[a] from entry No. 3 in Table 6.

Conductive polymers/zeolite (nano-)composites: sub-exploited materials

Mehdi Jaymand*

Research Center for Pharmaceutical Nanotechnology, Tabriz University of Medical Sciences, P.O. Box: 5165665811, Tabriz, IR, Iran.

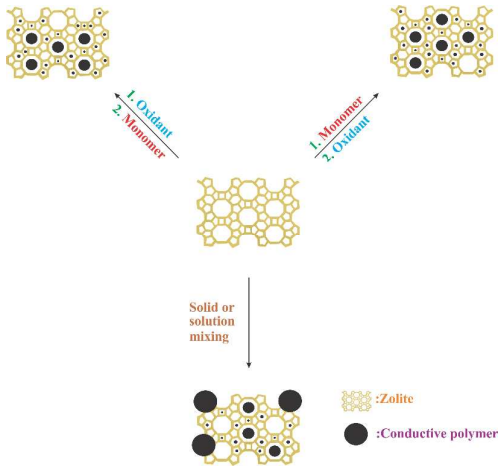

This review provides a snapshot of recent progress in the synthesis, materials properties, and applications of conductive polymers/zeolite (nano-)composites reported until March 2014.

* Correspondence to: Mehdi Jaymand, Research Center for Pharmaceutical Nanotechnology, Tabriz University of Medical Sciences, Tabriz, Iran

Tel: + 98-411-3367914; Fax: +98-411-3367929
Postal address: Tabriz-5165665811-Iran
E-mail addresses: m_jaymand@yahoo.com; m.jaymand@gmail.com; jaymandm@tbzmed.ac.ir